

**The role of TAK1 in regulation of  
ER stress and leptin resistance**

(小胞体ストレス及びレプチン抵抗性  
の制御における TAK1 の機能解析)

**Kazuhito Sai**

Division of Biological Science, Graduate  
School of Science, Nagoya University, Japan

## TABLE OF CONTENTS

### **Chapter I**

<b>TAK1 regulation of ER stress tolerance.....</b>	<b>3</b>
ABSTRACT.....	3
INTRODUCTION.....	4
RESULTS.....	6
DISCUSSION.....	11

### **Chapter II**

<b>Targeting TAK1 in HFD-induced leptin resistance and obesity.....</b>	<b>14</b>
ABSTRACT.....	14
INTRODUCTION.....	15
RESULTS.....	17
DISCUSSION.....	22

---

MATERIALS AND METHODS.....	25
ACKNOWLEDGEMENT.....	35
REFERENCES.....	36
FIGURES.....	45

## Chapter I

### TAK1 regulation of ER stress tolerance

#### ABSTRACT

Sustained endoplasmic reticulum (ER) stress disrupts normal cellular homeostasis and thus contributes to the development of many types of human diseases including metabolic disorders. Here we demonstrate that a member of the mitogen-activated protein kinase kinase kinase (MAPKKK) family TAK1 regulates ER stress tolerance through a previously uncharacterized mechanism in cultured cells. *Tak1*-deficient cells were more resistant to ER stress-induced cell death compared with wild type cells. Intriguingly, *Tak1* deficiency did not alter induction of unfolded protein responses (UPR), which are protective signaling cascades against ER stress. Instead, deletion of *Tak1* was found to increase ER volume through upregulation of sterol-regulatory element binding proteins (SREBPs)-dependent lipogenesis, which facilitated ER stress tolerance. These results revealed a previously unidentified function of TAK1 in ER stress regulation and provide a new approach to control cellular ER stress tolerance.

## INTRODUCTION

The endoplasmic reticulum (ER) is a large organelle that forms an interconnected network in the cytoplasm. The ER has two structurally distinct domains, the smooth and rough ER. The smooth ER is responsible for cellular detoxification and lipid synthesis, whereas the rough ER, characterized by the presence of ribosomes on the surface, plays a critical role in folding and transportation of newly synthesized secreted and membrane proteins (1, 2).

Given that approximately one-third of proteins are processed in the rough ER, this organelle is indispensable for the maintenance of cellular protein homeostasis. Secreted and membrane proteins are translated by ER-bound ribosomes and translocate into the ER lumen where they are subjected to covalent post-translational modifications, chaperone-mediated folding and transport toward their final destinations. Disruption of post-transcriptional modifications, expression of folding-defective mutant proteins or inhibition of ER chaperons result in accumulation of unfolded and misfolded proteins in the ER lumen leading to a condition known as ER stress. ER stress activates intracellular signaling pathways, collectively referred to as the unfolded protein response (UPR), which is initiated by three sensor/mediator proteins localized to ER membrane; protein kinase RNA-like endoplasmic reticulum kinase (PERK), inositol-requiring enzyme 1 (IRE1) and ATF6. UPR signaling transcriptionally activates expression of protein chaperon genes, pauses canonical protein synthesis and increases biogenesis of ER membrane, which upregulate ER functional capacity and accelerate the processing of accumulated proteins in the ER (3). However, if ER stress is unresolved and sustained, the UPR is switched

to activating signaling pathways that lead to caspase-dependent apoptosis (4, 5).

Transforming growth factor  $\beta$ -activated kinase 1 (TAK1) is a member of the mitogen activated kinase kinase kinase (MAPKKK) family that is a key signaling intermediate of proinflammatory signaling pathways (6, 7). TAK1 is activated by a diverse set of inflammatory stimuli, such as TNF and IL-1. Transcription factor NF- $\kappa$ B and the MAPK cascades are well-documented downstream targets of TAK1, which activate a number of genes promoting cell survival and inflammatory responses. *Tak1* deficiency is associated with hyper-sensitivity to TNF, Toll-like receptor ligand- and reactive oxygen species-induced cell death in fibroblasts, keratinocytes, macrophages, hepatocytes, intestinal epithelial cells and endothelial cells (7, 8). Tissue-specific deletion of *Tak1* results in profound cell death and tissue injury in the epidermis, intestinal epithelium, liver and endothelium (9-12). Thus, TAK1 has been recognized as a pro-survival factor. However, we found that *Tak1*-deficient cells are not always hypersensitive to cell killing stimuli, but they are rather resistant to certain types of stimuli such as ER stressors. In the present study, we investigated this previously unrecognized role of TAK1 in the ER stress regulation.

## RESULTS

### ***Tak1*-deficient cells are resistant to ER stress-induced cell death**

*Tak1* deficiency induces cell death in multiple tissues and TNF has been identified as a primary inducer of cell death in the epidermis, liver and endothelium (9, 10, 12). However, ablation of TNF signaling does not always block cell death in some tissues including the adult intestinal epithelium (13). To determine additional inducers of *Tak1* deficiency-dependent cell death, we initially tested several cell death-associated stimuli including ER stress inducers. We treated *Tak1*-deficient mouse fibroblasts with ER stress inducers, tunicamycin and thapsigargin, and monitored viability of control and *Tak1*-deficient cells at 18 h post ER stress induction. Unexpectedly, we found that *Tak1* deficiency did not decrease, but rather increased cell survival during ER stress exposure compared to wild-type fibroblasts (Fig. 1A, B). ER stress resistance was also observed in *Tak1*-deficient keratinocytes (Fig. 1C, D). Sustained ER stress is known to induce apoptosis through activation of caspases (5). We found that proteolytic cleavage of caspase-3 upon ER stress exposure was markedly attenuated in *Tak1*-deficient fibroblasts compared to control fibroblasts (Fig. 1E), indicating that *Tak1* deletion protected cells from ER stress-induced cell death. Resistance to ER stress-induced cell death can be due to alleviation of ER stress or alternative defects in apoptotic cell death pathways. However, as TNF stimulation induces caspases-dependent apoptosis in *Tak1*-deficient fibroblasts and keratinocytes (14, 15), *Tak1*-deficiency is likely to alleviate ER stress. Indeed, induction of *Chop* expression by ER stressor treatment, an indicator of prolonged/unresolved

ER stress (16), was reduced in *Tak1*-deficient cells (Fig. 1F), supporting the idea that *Tak1*-deficiency alleviated ER stress.

### ***Tak1* deficiency does not upregulates UPR**

To determine how TAK1 regulates ER stress, we first tested the possibility that TAK1 directly modulates signal transduction of the UPR. Since effective induction of UPRs can prevent ER stress-induced cell death (17), *Tak1* deficiency may upregulate UPRs. However, quantification of the levels of UPR-induced mRNAs (*Atf4*, *Xbp1S* and *Grp78*) upon ER stressor treatment did not reveal any clear trends of upregulation in UPRs in *Tak1*-deficient cells compared to wild-type cells (Fig. 2A-C). To further investigate UPRs in *Tak1* deficient cells, *Xbp1*-splicing and phosphorylation of PERK were examined. For *Xbp1*-splicing, unspliced-*Xbp1* (*Xbp1U*) and spliced form of *Xbp1* (*Xbp1S*) mRNAs were analyzed by reverse transcriptional PCR (Fig. 2D). *Xbp1*-splicing effectively occurred both in wild-type and *Tak1*-deficient cells upon ER stressor treatment, which generated *Xbp1S* at similar levels consistent with the results in real time PCR of *Xbp1S* shown in Fig. 2B. PERK phosphorylation was also found to be induced both in wild-type and *Tak1*-deficient cells and the levels of phosphorylation did not show increasing trends by *Tak1* deficiency (Fig. 2E). However, we found that the protein level of PERK in untreated *Tak1*-deficient cells was higher compared to wild-type cells (Fig. 2E, 2<sup>nd</sup> panels), which is discussed later in this section. These results suggest that ER stress resistance of *Tak1*-deficient cells is not due to upregulation of UPR signaling pathways.

### ***Tak1* deficiency increases ER volume**

Intriguingly, in the course of UPR signaling analysis, we realized the amounts of ER resident proteins, including PERK, IRE1 $\alpha$  and calnexin were basally elevated in *Tak1*-deficient fibroblasts (Fig. 3A and Fig. 2E, 2<sup>nd</sup> panels). Since expression levels of ER resident proteins are coordinately regulated with ER volume (18), this prompted us to test the possibility that ER volume may be increased in *Tak1*-deficient cells. To visualize the ER, we utilized the ER retention signal motif, KDEL, which is included in multiple ER resident proteins and widely used to assess ER distribution (19). Immunofluorescence staining of KDEL motif-containing proteins revealed that ER volume was indeed markedly increased in *Tak1*-deficient fibroblasts compared to wild-type fibroblasts (Fig. 3B and C), which was confirmed by the immunoblotting detecting KDEL motif-containing proteins (Fig. 3D). Consistent with elevation of KDEL proteins, electron microscopic analysis demonstrated that the membranous structure of the rough ER, determined by membrane-bound ribosomes, was pronouncedly elongated and distributed throughout the cytoplasm of *Tak1*-deficient fibroblasts (Fig. 3E). ER volume is primarily regulated by ER membrane biogenesis (20), and proliferation of ER membrane is known to upregulate the functional capacity of ER resulting in ER stress resistance (21). Thus, *Tak1*-deficiency alleviates ER stress and protects cells potentially by increasing ER membrane biogenesis.

### ***Tak1* deficiency increases ER volume and ER stress tolerance by upregulating SREBPs**

Next, we examined whether *Tak1* deletion increases ER volume by upregulating ER membrane biogenesis. Membrane lipids are generated through lipogenesis, in which sterol regulatory element-binding proteins

(SREBPs), SREBP1 and SREBP2, transcriptionally regulate the expression of lipogenic enzymes (22). We recently found that TAK1 directly binds to and inhibits SREBPs, and that deletion of *Tak1* upregulates lipogenic enzymes in the mouse liver (23). This raises the possibility that TAK1 regulates ER membrane biogenesis and ER stress tolerance through SREBPs. We observed that SREBP target lipogenic enzymes, *acetyl-CoA carboxylase1* (*Acc1*), *glycerol-3-phosphate acyltransferase* (*Gpat*) and *mevalonate kinase* (*Mvk*) were significantly upregulated in *Tak1*-deficient cells. *Fatty acid synthase* (*Fasn*) and *stearoyl coenzyme-A desaturase1* (*Scd1*) also showed an increasing trend, although the differences did not reach statistical significance (Fig. 4A). To investigate whether deletion of *Tak1* increases lipid synthesis, we conducted a lipid fluxomics analysis. While we observed little incorporation of  $^{13}\text{C}$  into palmitic acid (supplementary Fig. S1B) and stearic acid (supplementary Fig. S1C) in wild-type cells during 12 h incubation with  $[1,2-^{13}\text{C}]$ acetate, we detected significantly increased incorporation of  $^{13}\text{C}$  into those fatty acids in *Tak1*-deficient cells. These results suggest that, while de novo lipid synthesis pathway is normally very low in cultured fibroblasts, *Tak1* deficiency indeed enhances de novo fatty acid synthesis. To determine the causal relationship between upregulation of SREBPs and ER stress resistance in *Tak1*-deficient fibroblasts, we introduced siRNAs targeting *Srebp1* and *Srebp2* into *Tak1*-deficient fibroblasts. mRNA levels of *Srebp1* and *Srebp2* were effectively reduced by the siRNA transfection, which resulted in attenuation of *Fasn*, *Scd1*, *Acc1*, *Gpat* and *Mvk* expression levels (supplementary Fig. S1D). Immunoblotting for KDEL-containing proteins demonstrated that depletion of *Srebps* in *Tak1*-deficient cells reduced the amount of ER resident proteins at a level similar to that in wild-type cells

(Fig. 4B). Under this condition, ER stress tolerance of *Tak1*-deficient cells was restored to a level comparable with wild-type cells (Fig. 4C). To further confirm that SREBPs are important for *Tak1* deficiency-induced ER stress resistance, we treated *Tak1*-deficient cells with fatostatin, a pharmacological inhibitor of SREBPs (24). Consistently, fatostatin reduced the ER stress tolerance in *Tak1*-deficient fibroblasts (Fig. 4D). Taken together, these results demonstrate that TAK1 negatively regulates ER membrane biogenesis and ER stress tolerance by inhibiting SREBPs, and that deletion of *Tak1* alleviates ER stress by upregulating SREBPs-dependent ER membrane biogenesis.

## DISCUSSION

### Identification of SREBPs as mammalian regulators of ER membrane biogenesis

The ER is a highly dynamic organelle that changes its membranous structure and volume under certain situations. It has long been known that exposure to xenobiotics, such as 1,4-bis[2-(3,5 dichloropyridyloxy)] benzene (TCPOBOP), induces proliferation of ER membrane and enhances cellular detoxification ability (25, 26). B cell differentiation requiring high-rate protein secretion is accompanied by increased biogenesis of ER membrane (18). ER stress is also known to induce ER proliferation, which increases ER functional capacities to attenuate ER stress (20). In yeast, ER stress activates INO2/4 transcription factor complex, an important regulator of phospholipid synthesis, to upregulate ER membrane biogenesis and ER proliferation (21). However, since INO2/4 are not conserved in mammals, the regulatory molecular mechanism of ER membrane synthesis is still undetermined in mammals (27). Our unexpected finding that *Tak1* deficiency protects cells from ER stress led us to investigate the mechanism of TAK1 regulation of ER function. Here we show that ER proliferation is the cause of ER stress resistance of *Tak1*-deficient cells, which is mediated by upregulation of SREBPs-dependent membrane lipid biogenesis. This indicates that SREBPs are previously unidentified regulators of ER membrane synthesis in mammals, which increase ER volume and protect cells from ER stress-induced cell injury. This notion is consistent with a recent report showing that depletion of SREBPs alters ER membrane lipid composition and causes ER stress in cultured cells (28).

**Physiological role of TAK1 regulation of SREBPs**

Lipid metabolism and innate immune response are closely related, as studies revealed that inflammation alters lipid metabolism in many tissues including the liver and macrophages (29). The change in lipid metabolism during inflammation is considered as an important regulator of immune responses. Circulating free fatty acid (FFA) is known to be elevated during inflammation, which amplifies inflammatory responses by, at least partially, activation of Toll-like receptors (TLRs) signaling (29). Hypercholesterolaemia induces cholesterol overload in macrophages, which triggers inflammatory responses and worsens inflammatory disorders such as atherosclerosis (30, 31). These studies depict the reciprocal interaction between lipogenesis and inflammation, which seemingly form a positive feedback regulation. Thus, regulation of SREBP is associated with not only lipid homeostasis but also inflammation. TAK1 is activated under inflammatory conditions, and in turn triggers multiple downstream pathways leading to production of inflammatory mediators (8). Our current study has newly revealed that SREBPs are the additional downstream of TAK1. What is the physiological role of TAK1 regulation of SREBPs? A possible explanation is that TAK1 regulation of SREBPs may function as a negative feedback regulator of lipogenesis during inflammation. Since lipid accumulation has deleterious effects in multiple cell types/tissues such as the liver, skeletal muscle and macrophages, lipid metabolism need to be tightly regulated (30). Indeed, our recent findings show that liver-specific deletion of *Tak1* results in over-activation of SREBPs and hepatic steatosis (23), implying the importance of TAK1-dependent suppression of excess lipogenesis. Alternatively, this regulation may provide a backup mechanism for innate immune system during

pathogen infection. A number of pathogenic bacteria and viruses are reported to have proteins that inhibit TAK1 complex to attenuate inflammation for their survival and effective proliferation (6). If inhibition of TAK1 results in activation of SREBPs-dependent lipogenesis, it might be beneficial to facilitate inflammatory responses to compensate for the absence of TAK1-mediated inflammation. This also explains why *Tak1* deficiency induces ER expansion, as it may enhance the secretory capacity of proinflammatory cytokines (32).

## Chapter II

### Targeting TAK1 in HFD-induced leptin resistance and obesity

#### ABSTRACT

ER stress is associated with multiple human diseases. Chronic ingestion of high-fat diet (HFD) is known to induce ER stress in the hypothalamic neurons, which impairs leptin signaling and results in hyperphagic obesity. Thus, amelioration of hypothalamic ER stress is a promising strategy for prevention of obesity; however, effective approaches to modulate ER stress are limited. Since *Tak1* deficiency alleviates ER stress in cultured cells, we reasoned that targeting TAK1 in the hypothalamic neurons might improve HFD-induced leptin resistance by attenuating ER stress. Using mouse fibroblasts ectopically expressing leptin receptors, we confirmed that *Tak1* deficiency indeed blocked ER stress-induced leptin resistance monitored by leptin-induced phosphorylation of STAT3. Central nervous system (CNS)-specific *Tak1* deletion upregulated SREBP target lipogenic genes and blocked ER stress in mouse hypothalamus as it does in cultured cells. Furthermore, CNS-specific *Tak1* deletion prevented ER stress-induced hypothalamic leptin resistance and hyperphagic obesity under HFD. Thus, TAK1 is a critical regulator of ER stress *in vivo*, which could be a target for alleviation of ER stress and its associated disease conditions.

## INTRODUCTION

Emerging evidence suggests that ER stress contributes to the development of a diverse set of human diseases including neurodegenerative and inflammatory diseases (33, 34). Specifically, ER stress is known to be causally associated with the development of metabolic disorders such as obesity and type II diabetes, which can be initiated by chronic ER stress in multiple tissues including the liver, adipose tissues and the hypothalamus (35-37). High-fat diet (HFD)-induced obesity is a well-characterized ER stress-associated disorder in mouse models. Under normal conditions, feeding stimulates secretion of a satiety hormone, leptin, from adipose tissues. Circulating leptin binds to its receptors, activating neurons of the arcuate nucleus within the hypothalamus (specifically POMC and AgRP neurons), leading to appetite suppression (38, 39). Chronic HFD is known to induce ER stress and impairs leptin signaling in the hypothalamus, which results in the conditions known as leptin resistance and hyperphagic obesity (40).

The causal relationship between ER stress and hypothalamic leptin resistance has been demonstrated by a series of mouse studies (40-42), and thus targeting ER stress in the hypothalamus is a promising strategy to treat HFD-induced metabolic dysfunctions. Nonetheless, the practical method to alleviate ER stress in human patients is still limited. Intracerebroventricular administration of chemical chaperons, such as 4-phenylbutyrate (4-PBA) and tauroursodeoxycholic acid (TUDCA) are known to improve HFD-induced obesity and several neurodegenerative diseases in the mouse models (40, 43), yet their effects on human diseases are not determined and their lack of substrates specificity is likely to be problematic (44). This has

inspired recent chemical screens that have identified compounds which improve ER functions and can reverse metabolic dysfunctions in the mouse model (45, 46).

As discussed in chapter I, we found that *Tak1* deficiency induces ER expansion and protects cells from ER stress. This finding prompted us to examine whether targeting TAK1 in ER stress-associated diseases would improve disease outcomes. Using neuron-specific *Tak1* knockout mice system, we asked whether TAK1 deficiency protects mice against HFD-induced leptin resistance and the subsequent development of hyperphagic obesity.

## RESULTS

### ***Tak1* deficiency protects cells from ER stress-induced leptin resistance**

Prolonged ER stress disrupts cellular homeostasis and is known to be associated with the development of various human diseases. The central nervous system (CNS) is highly susceptible to ER stress, which is illustrated by the fact that chronic ER stress is causally associated with many types of neurodegenerative diseases and neuron-derived metabolic disorders (47, 48). Our results described above demonstrate that *Tak1* deficiency alleviates ER stress in cultured cells, which led us to examine the possibility that inhibition of TAK1 improves pathology of ER stress-associated neuronal disorders. An adipose tissue-derived hormone, leptin is the central regulator of appetite by targeting appetite-associated hypothalamic neurons and activating the intracellular JAK2-STAT3 signaling pathway leading to feeding suppression (49). Chronic ingestion of HFD is known to induce ER stress in hypothalamic neurons, which inhibits leptin-induced STAT3 activation and impairs proper appetite control (40). To test whether *Tak1* deficiency is protective against ER stress-induced blockade of leptin signaling, we first utilized *Tak1*-deficient fibroblasts expressing exogenously introduced leptin receptor b, and monitored leptin-induced STAT3 phosphorylation in the presence and absence of an ER stressor tunicamycin. Whereas 8 h-treatment of tunicamycin significantly diminished leptin-induced STAT3 phosphorylation in wild-type fibroblasts, tunicamycin-treated *Tak1*-deficient fibroblasts still responded to leptin (supplementary Fig. S2A, B). This suggests that *Tak1* deficiency indeed prevents ER stress-induced leptin resistance in cultured cells.

### **CNS-specific deletion of *Tak1* activates SREBPs and induces ER expansion in the hypothalamus**

To test whether *Tak1* deficiency prevents ER stress-induced leptin resistance *in vivo*, we generated CNS-specific *Tak1*-deficient mice (hereafter referred to as *Tak1*<sup>nKO</sup> mice) by crossing *Tak1*<sup>flox/flox</sup> mice to a *Nestin-Cre* transgenic line that is widely used to achieve gene deletion in the CNS (36, 50). In *Tak1*<sup>nKO</sup> mice, the levels of TAK1 protein in the CNS were reduced at embryonic day 18.5 and effectively diminished by postnatal day 12 (supplementary Fig. S3A), as *Nestin-Cre* system effectively directs recombination starting from late embryonic period (51). As heterozygous CNS-specific *Tak1* deletion (*Tak1*<sup>flox/+</sup> *Nestin-Cre*) did not reduce TAK1 protein levels (supplementary Fig. S3A), we used wild-type (*Tak1*<sup>flox/flox</sup> no-*Cre*) and *Tak1*<sup>flox/+</sup> *Nestin-Cre* littermate or age-matched mice as controls for *Tak1*<sup>nKO</sup> mice. Consistent with a recent report (52), *Tak1*<sup>nKO</sup> mice exhibited no overt abnormalities during our experimental period up to 12 months. There were no detectable differences in the amount of food intake (supplementary Fig. S3B), body temperature (supplementary Fig. S3C) and percent visceral fat (supplementary Fig. S3D) between control and *Tak1*<sup>nKO</sup> mice under normal diet feeding. We first examined whether *Tak1* deficiency in the CNS increases SREBPs activities and ER volume as it does in fibroblasts. Indeed, SREBP target genes, *Srebp1*, *Srebp2*, *Scd1*, *Gpat* and *Mvk* were significantly upregulated in the hypothalamus of *Tak1*<sup>nKO</sup> mice (Fig. 5A). We also detected a moderate increase of *Fasn* and *Acc1* expression levels. Double-immunofluorescence staining of neuronal marker neurofilament 200 and KDEL containing proteins in the hypothalamus demonstrated that ER volume was increased

in the hypothalamic neurons of *Tak1*<sup>nKO</sup> mice (Fig. 5B), which was confirmed by immunoblotting of the hypothalamic extracts (Fig. 5C). We then asked whether *Tak1*-deficient hypothalamic neurons are resistant to ER stress. We injected tunicamycin into the third ventricle of *Tak1*<sup>nKO</sup> and control mice, which is known to induce ER stress in the hypothalamus (40). We observed ER stress-induced activation of UPRs both in control and *Tak1*<sup>nKO</sup> hypothalamus. Consistent with the UPRs observed in cultured fibroblasts, *Xbp1*-splicing occurred at comparable levels between control and *Tak1*<sup>nKO</sup> hypothalamus (supplementary Fig. S4A). We also examined PERK phosphorylation by detecting a retarded PERK migration on SDS-PAGE (supplementary Fig. S4B, top panel). Tunicamycin injection induced a shift in PERK migration in both control and *Tak1*<sup>nKO</sup> hypothalamus. These slower migrating smear bands were diminished by phosphatase treatment, indicating these are phosphorylated forms of PERK. We note here that the intensity of phosphorylated PERK bands was much lower in the hypothalamic PERK compared to that in fibroblasts (see Fig. 2E), and we were not able to detect phosphorylated PERK with anti-phospho-PERK antibody in the hypothalamus. PERK activation may be weaker in the hypothalamus compared to fibroblasts under our experimental settings. In this context, caspase-3 cleavage was slightly induced in the control hypothalamus (supplementary Fig. S4B, 2<sup>nd</sup> panel). We found that the caspase-3 cleavage was completely attenuated by *Tak1*-deficiency (supplementary Fig. S4B, 2<sup>nd</sup> panel), suggesting that *Tak1* deficiency alleviates ER stress in the hypothalamus without altering UPRs as does in cultured fibroblasts.

### **CNS-specific deletion of *Tak1* protects mice against ER stress-induced leptin resistance**

We then examined whether *Tak1* deletion improves ER stress-induced leptin resistance *in vivo*. We injected tunicamycin into the third ventricle of the brain of *Tak1*<sup>nKO</sup> and control mice, and subsequently leptin was administered to the mice by intraperitoneal (ip) injection. As expected, while leptin injection effectively induced STAT3 phosphorylation in the hypothalamus of untreated mice (Fig. 6A), tunicamycin infusion completely blocked leptin-induced STAT3 phosphorylation in the hypothalamus of control mice (Fig. 6B, lanes 1-4). In contrast, tunicamycin failed to block leptin-induced STAT3 phosphorylation in the hypothalamus of *Tak1*<sup>nKO</sup> mice (Fig. 6B, lane 5-9), suggesting that deletion of *Tak1* alleviates ER stress and prevents leptin resistance in both *in vitro* and *in vivo* settings.

### **CNS-specific deletion of *Tak1* protects mice against HFD-induced leptin resistance and hyperphagic obesity**

As *Tak1* deletion prevented ER stress-induced leptin resistance, we next asked whether *Tak1* deficiency in the CNS protects mice against HFD-induced leptin resistance and subsequent obesity. To this end, we placed 4-week-old mice on a HFD for 12 weeks, and examined leptin sensitivity in the hypothalamus. While ip injection of leptin effectively induced STAT3 phosphorylation in the hypothalamus of normal diet-fed control mice (Fig. 7A, lanes 1-4), the effect of leptin was much smaller in HFD-fed control mice (Fig. 7A, lanes 5-7). This indicates that HFD-ingestion induced leptin resistance in control mice in our experimental paradigm. In contrast, leptin injection effectively induced STAT3 phosphorylation in the hypothalamus

of HFD-fed *Tak1*<sup>nKO</sup> mice (Fig. 7A, lane 8-12). Consistent with this finding, while ip injection of leptin failed to suppress food intake of HFD-fed wild-type mice, leptin effectively suppressed food intake of HFD-fed *Tak1*<sup>nKO</sup> mice (Fig. 7B). These results clearly demonstrate that mice lacking CNS *Tak1* did not develop leptin resistance under HFD feeding. Furthermore, whereas HFD feeding markedly increased body weight of control mice compared to normal diet feeding, *Tak1*<sup>nKO</sup> mice showed marked resistance to HFD-induced excessive weight-gain (Fig. 7C). This protective effect against HFD feeding was not observed in mice having heterozygous CNS-specific *Tak1* deletion (*Tak1*<sup>fllox/+</sup> *Nestin-Cre*) (supplementary Fig. S3F), demonstrating that expression of *Nestin-Cre* alone did not cause observable effects under our experimental settings, although several earlier studies report marginal reductions in weight gain by *Nestin-Cre* expression (53). Thus, CNS-specific *Tak1* deletion is the cause of resistance to HFD-induced excessive weight gain. Accordingly, adiposity of HFD-fed *Tak1*<sup>nKO</sup> mice was smaller than that of control mice (Fig. 7D). As expected, HFD-fed *Tak1*<sup>nKO</sup> mice showed slightly reduced circulating leptin levels compared to HFD-fed control mice, as it reflects body fat levels, although the difference in the leptin levels did not reach statistic significance (supplementary Fig. S3E). Consistent with the improved leptin sensitivity, food intake of HFD-fed *Tak1*<sup>nKO</sup> mice was significantly lower than that of control mice (Fig. 7E). These results demonstrate that deletion of *Tak1* in the CNS can prevent HFD-induced leptin resistance and hyperphagic obesity, which is likely due to improved ER function.

## DISCUSSION

### **SREBPs as new signaling intermediates of TAK1 *in vivo***

In the present study, we show that targeting TAK1 in the hypothalamus can improve HFD-induced leptin resistance and obesity by alleviating ER stress. TAK1 is an intracellular signaling intermediate activated by inflammatory stimuli, which functions to transmit a signal from the receptor proximal molecules such as a complex of TNF receptor, TNF receptor activated factors (TRAFs), and receptor interacted protein kinase 1 (RIPK1) to downstream signaling cascades such as I $\kappa$ B kinase-NF- $\kappa$ B and MAPKK-MAPKs (7). Interestingly, hypothalamic NF- $\kappa$ B and JNK are known to be activated upon HFD ingestion, and ablation of NF- $\kappa$ B or JNK also improves HFD-induced leptin resistance (36, 54, 55). This raises the possibility that *Tak1* deficiency may reduce activity of NF- $\kappa$ B and/or JNK in the hypothalamus, which could participate in protection of leptin resistance. We found that HFD ingestion activated TAK1 and JNK in the hypothalamus (supplementary Fig. S5A). However, JNK activity was not altered by *Tak1* deletion (supplementary Fig. S5B), hence JNK is unlikely to be the downstream of TAK1 in the hypothalamus. In contrast, NF- $\kappa$ B activity, monitored by electrophoresis mobility shift assay (EMSA) (supplementary Fig. S5A) and phosphorylation of p65 (supplementary Fig. S5B), was not detectably upregulated in our experimental settings even under the condition where TAK1 was activated. Our detection efficiency of NF- $\kappa$ B activation may be lower than that in the earlier study (36). Nonetheless, *Tak1* deficiency altered neither DNA-binding activity of NF- $\kappa$ B (supplementary Fig. S5A) nor p65 phosphorylation (supplementary Fig. S5B). We note here that endothelial-specific *Tak1* deletion also does not

alter NF- $\kappa$ B activity in the blood vessels (12). Collectively, TAK1 signaling is not always associated with JNK and NF- $\kappa$ B *in vivo*, which is consistent with the fact that ablation of NF- $\kappa$ B or MAPKs does not result in the similar tissue abnormalities as those in *Tak1*-deficient tissue (7, 56-58). We conclude that TAK1 regulation of lipogenesis, but not NF- $\kappa$ B or JNK, is involved in hypothalamic alterations in CNS-specific *Tak1*-deficient mice. Our results reveal that SREBP-dependent lipogenesis is the previously unrecognized target of TAK1 and it may be a critical downstream of TAK1 not only in the brain but also in other tissues, which warrant further investigations.

### **Targeting TAK1 in ER stress-associated human diseases**

In the present study, we demonstrate that deletion of *Tak1* protects cells from ER stress both in the *in vitro* cell culture system and in the CNS. Importantly, *Tak1*<sup>nKO</sup> mice did not show overt histopathological abnormalities and pharmacological inhibition of TAK1 in the brain was reported not to cause adverse effects but rather to be associated with resistance in the murine model of cerebral ischemia and experimental traumatic brain injury (59, 60). Thus, TAK1 is likely to be a low risk target for therapeutic approaches in the brain. Our finding revealed that TAK1-SREBP regulation of ER membrane biogenesis is critically involved in susceptibility to ER stress, which raises the possibility that targeting TAK1 may be an alternative and suitable therapeutic approach to treat ER stress-associated neuronal diseases.

### **Does TAK1 link HFD-induced inflammation and ER stress?**

Chronic inflammation is one of the fundamental pathological processes associated with a number of human diseases, including neurodegenerative diseases, metabolic disorders and cardiovascular pathologies, which are often accompanied by ER stress (34, 36, 61-64). However, the molecular mechanism linking inflammation and ER stress is poorly understood. Here we demonstrate that TAK1 negatively regulates cellular ER stress tolerance by inhibiting SREBP-dependent ER membrane biogenesis. Given that TAK1 is activated by a diverse set of inflammatory stimuli including IL-1 and TNF, one possible mechanism linking inflammation and ER stress is that activation of TAK1 by inflammatory cytokines inhibits ER membrane biogenesis through downregulation of SREBP-dependent lipogenesis, that results in functional impairment of the ER. Indeed, our data demonstrate that HFD feeding, an inducer of inflammation in the hypothalamus (65), activated hypothalamic TAK1 (see supplementary Fig. S5A), and that deletion of *Tak1* in the CNS blocked ER stress-induced leptin resistance. We propose that TAK1 activation may be a previously uncharacterized link between inflammation and ER stress in the context of human diseases.

## MATERIALS AND METHODS

### Mice and cell culture

*Tak1*-floxed (*Tak1*<sup>flox/flox</sup>) mice and *Tak1*-deficient fibroblasts have been described previously (8). *Nestin-Cre* transgenic mice were obtained from the Jackson Laboratories (66). All strains used were backcrossed at least 7 times to C57BL/6. *Tak1*-deficient keratinocytes were described previously (9). Littermate and age-matched wild type (*Tak1*<sup>flox/flox</sup> no-*Cre*) and heterozygous *Tak1* deletion (*Tak1*<sup>flox/+</sup> *Nestin-Cre*) mice, which were phenotypically indistinguishable, were used as control in all mouse experiments. Mouse embryonic fibroblasts were cultured in Dulbecco's modified Eagle's medium supplemented with 10% bovine growth serum (Hyclone) and penicillin-streptomycin at 37 °C in 5% CO<sub>2</sub>. Keratinocytes were cultured in Ca<sup>2+</sup>-free Eagle's minimal essential medium (BioWhittaker) supplemented with 4% Chelex-treated bovine growth serum, 10 ng/ml of human epidermal growth factor (Invitrogen), 0.05 mM calcium chloride, and penicillin-streptomycin at 33°C in 8% CO<sub>2</sub>. 60% calories from fat (high fat) diet (D12492, Research Diets) and 13.4 kcal% fat control diet (5001, Lab Diet) were used. To test leptin sensitivity, 1 µg/g body weight of recombinant murine leptin (Pepro Tech) was injected intraperitoneally. All animal experiments were conducted according to protocols approved by the North Carolina State University Institutional Animal Care and Use Committee.

### Plasmids and reagents

Leptin receptor b-expressing plasmid was described previously (40). Plasmids were transfected to the cells using TransIT-X2 Reagent (Mirus

Bio LLC). Tunicamycin, thapsigargin and fatostatin were purchased from Millipore. Pst I restriction enzyme was purchased from New England Biolabs.

### **Crystal violet assay**

Cells were plated on 24-well dishes 24 h prior to staining, at a concentration of  $2 \times 10^4$  cells per well. Cells were treated with either tunicamycin or thapsigargin for 18 h. For fatostatin treatment, cells are pretreated with 10  $\mu\text{g/ml}$  of fatostatin 24 h prior to ER stress induction. Cells were then washed with PBS and fixed in 10% formalin, and stained with 0.1% crystal violet. The dye was eluted in 50 % ethanol, 0.1 M sodium citrate and analyzed at 595 nm using SmartSpec<sup>TM</sup> 3000 (Bio-Rad).

### **Immunoblotting**

Protein extracts from fibroblasts and the hypothalamus were prepared using an extraction buffer containing 20 mM Hepes, pH 7.4, 150 mM NaCl, 12.5 mM  $\beta$ -glycerophosphate, 1.5 mM  $\text{MgCl}_2$ , 2 mM EGTA, 10 mM NaF, 2 mM DTT, 1 mM  $\text{Na}_3\text{VO}_4$ , 1 mM phenylmethylsulfonyl fluoride, 20  $\mu\text{M}$  aprotinin, and 0.5% Triton X-100. The extracts were resolved on SDS-PAGE and transferred onto Hybond-P PVDF membranes (GE Healthcare). The membranes were then immunoblotted with the indicated antibodies, and the bound antibodies were visualized with horseradish peroxidase-conjugated antibodies against rabbit or mouse IgG using the ECL Western blotting system (GE Healthcare, 1:10000). Primary antibodies used are; Anti-TAK1 antibody was described previously (67) (1:500). Anti-phospho-TAK1 (Thr187) (Cell Signaling Technology, 1:1000), Anti- $\beta$ -actin (Sigma, AC15, 1:1000), Anti-PERK (Cell Signaling Technology,

C33E10, 1:1000), Anti-phospho-PERK (Thr980) (Cell Signaling Technology, 16F8, 1:1000), Anti-IRE1 $\alpha$  (Cell Signaling Technology, 14C10, 1:1000), Anti-calnexin (Santa Cruz Biotechnology, H-70, 1:200), Anti-KDEL (ENZO, 10C3, 1:1000), Anti-STAT3 (Cell Signaling Technology, D1A5, 1/1000), Anti-phospho-STAT3 (Tyr705) (Cell Signaling Technology, D3A7, 1:2000), anti-JNK1/2 (Santa Cruz Biotechnology, sc571, 1:200), Anti-phospho-JNK (Thr183/Tyr185) (Cell Signaling Technology, #9251, 1:1000), anti-phospho-p65 NF- $\kappa$ B (Ser276) (Cell Signaling Technology, 1:1000) and Anti-p65 (Santa Cruz Biotechnology, C20, 1:1000). Intensities of each blotting were quantified using the ImageJ software.

### **Phosphatase treatment and PERK immunoblotting**

To dephosphorylate proteins, protein extracts were incubated with antarctic phosphatase (New England Biolabs) at 30 °C for 30 min. To determine PERK phosphorylation, protein extracts treated with/without phosphatase were separated in a 7% polyacrylamide gel and analyzed by immunoblotting.

### **Immunofluorescence microscopy analysis of fibroblasts**

Fibroblasts were seeded on glass coverslips in 6-well plates 24 h prior to fixation. Cells were fixed with 100% methanol for 2 min at -20°C, blocked with PBS containing 3% bovine serum albumin (Santa Cruz Biotechnology) for 30 min at room temperature, and then incubated with anti-KDEL antibody (ENZO, 10C3, 1:1000) followed by incubation with anti-mouse IgG conjugated with Alexa 594 (1:500). The coverslips were mounted with 50% glycerol and were examined by a fluorescence

microscope (model BX41; Olympus) and camera (model XM10; Olympus) at room temperature. For quantification of KDEL area, 3 randomly photographed pictures with the same exposure time were used. Each picture contains more than 70 cells, and KDEL-staining area was quantified using the ImageJ software. To calculate the average ER volume in a single cell, the total KDEL-staining area was divided by the cell number.

### **Immunofluorescence microscopy analysis of hypothalamic sections**

Mice were euthanized by CO<sub>2</sub> inhalation. The brains were rapidly removed and fixed with 4% paraformaldehyde at room temperature for 3 h. The brains were then transferred to 20% sucrose and kept at 4 °C for overnight. The brains were embedded in optimum cutting temperature (OCT) compound and frozen immediately. Cryosections (8 µm) were post-fixed with 100% methanol for 1 min at room temperature and blocked with PBS containing 3% bovine serum albumin for 30 min at room temperature, and then incubated with anti-KDEL antibody (ENZO, 10C3, 1:500) and anti-Neurofilament 200 (Sigma, 1:200) followed by incubation with anti-mouse IgG conjugated with Alexa 488 (1:500) and anti-rabbit IgG conjugated with Alexa 594 (1:500). The sections were stained with DAPI and the coverslips were mounted with 50% glycerol and were examined by a fluorescence microscope (model BX41; Olympus) and camera (model DP80; Olympus) at room temperature.

### **Electron microscopy analysis**

Fibroblasts were seeded on 100 mm dishes 24 h prior to fixation. Cells were fixed in Karnovsky's fixative, 2% paraformaldehyde (EM grade,

Electron Microscopy Sciences) and 2.5% glutaraldehyde (EM grade, Electron Microscopy Sciences) in PBS for over-night at 4°C, and subsequently post-fixed in 2% OsO<sub>4</sub> for 1 hour at 4°C in the dark. Cells were embedded in 2% agarose, dehydrated, and thin-sectioned on a Leica UC6rt (Leica Microsystems) at 80nm thickness on a DDK diamond knife (Delaware Diamond Knives). Sections were stained with both 4% aqueous uranyl acetate and Reynold's lead citrate prior to viewing on a JEOL JEM-1200EX TEM (JEOL USA) at 80 kV. Images were collected on Kodak 4489 film (Eastman Kodak), which was then scanned at 1200dpi using an Epson Perfection 4870 Photo flatbed scanner (Epson America). Digital images were then processed and labeled using Photoshop CS5.1 (Adobe Systems).

### Quantitative real time PCR Analysis

Total RNA was isolated from fibroblasts and the hypothalamic using Trizol (Invitrogen) or RNeasy kit (Qiagen) respectively, and transcribed into cDNA using MultiScribe reverse transcriptase (Life Technology). Expression level of *Chop*, *Atf4*, *Xbp1S*, *Grp78*, *Srebp1*, *Srebp2* and SREBP target genes were determined by quantitative real time PCR (qPCR) and normalized to the level of *Gapdh*. The following primers were used: *Chop*-forward, 5'-CAGGAAACGAAGAGGAAGAATCAA-3'; *Chop*-reverse, 5'-GCTTTGGGATGTGCGTGTGA-3'; *Atf4*-forward, 5'-ATGGCCGGCTATGGATGAT-3'; *Atf4*-reverse, 5'-CGAAGTCAAACCTCTTTCAGATCCATT-3'; *Xbp1S*-forward, 5'-GAGTCCGCAGCAGGTG-3'; *Xbp1S*-reverse, 5'-GTGTCAGAGTCCATGGGA-3'; *Grp78*-forward, 5'-GACTGCTGAGGCGTATTTGG-3'; *Grp78*-reverse, 5'-

AGCATCTTTGGTTGCTTGTCG-3';	<i>Srebp1</i> -forward,	5'-
GATCAAAGAGGAGCCAGTGC-3';	<i>Srebf1</i> -reverse,	5'-
TAGATGGTGGCTGCTGAGTG-3';	<i>Srebf2</i> -forward,	5'-
GGATCCTCCCAAAGAAGGAG-3';	<i>Srebf2</i> -reverse,	5'-
TTCCTCAGAACGCCAGACTT-3';	<i>Fasn</i> -forward,	5'-
AAGGCTGGGCTCTATGGATT-3';	<i>Fasn</i> -reverse,	5'-
GGAGTGAGGCTGGGTTGATA-3';	<i>Scd1</i> -forward,	5'-
CTGACCTGAAAGCCGAGAAG-3';	<i>Scd1</i> -reverse,	5'-
GCGTTGAGCACCAGAGTGTA-3';	<i>Acc1</i> -forward,	5'-
TGTTGGGAGTTGTGTGTGGG-3';	<i>Acc1</i> -reverse,	5'-
AGTGTGTGAGCAGGAAGGAC-3';	<i>Gpat</i> -forward,	5'-
CAACACCATCCCCGACATC-3';	<i>Gpat</i> -reverse,	5'-
GTGACCTTCGATTATGCGATCA-3';	<i>Mvk1</i> -forward,	5'-
GGGACGATGTCTTCCTTGAA-3';	<i>Mvk1</i> -reverse,	5'-
GAACTTGGTCAGCCTGCTTC-3';	<i>Gapdh</i> -forward,	5'-
GAAGGTCGCTGTGAACGGA-3';	<i>Gapdh</i> -reverse,	5'-
GTTAGTGGGGTCTCGCTCCT-3'.		

### ***Xbp1*-splicing assay**

Unspliced and spliced forms of *Xbp1* were amplified from cDNA using following primers. *Xbp1*-forward, 5'- CCTTGTGGTTGAGAACCAGG-3'; *Xbp1*-reverse, 5'- CTAGAGGCTTGGTGTATAC-3'. This results in production of unspliced *Xbp1* (*Xbp1U*, 451 bp), spliced *Xbp1* (*Xbp1S*, 425 bp) and a hybrid of unspliced/spliced *Xbp1* (*Xbp1H*, about 500 bp) DNA fragments. To clearly distinguish the DNA fragments of unspliced and spliced *Xbp1*, PCR products were incubated with Pst I restriction enzyme, which specifically digests unspliced *Xbp1*, at 37 °C for over-night. PCR

products were then separated by electrophoresis in a 2.5% agarose gel and visualized by ethidium bromide staining.

### **<sup>13</sup>C lipid fluxomics analysis**

Wild-type and *Tak1*-deficient fibroblasts were plated at  $5 \times 10^6$  per 100 mm plates, and incubated with 4 mM [1,2-<sup>13</sup>C] acetate (Sigma) for 0 or 12 h. Cells are then washed with 150 mM ammonium acetate and quenched in liquid nitrogen. Lipids were extracted and analyzed by GC-MS (Agilent 69890N GC -5975 MS detector). Metabolites were identified by matching the retention time and mass to authentic standards. Isotope peak areas were integrated using MassHunter Quantitative Analysis vB.07.00 (Agilent Technologies). Peak areas were corrected for natural isotope abundance, and data were normalized to cell protein content prior to analysis of metabolite fluxes for fatty acid metabolites. The lipogenic flux is shown with the percentages of palmitic and stearic (16:0 and 18:0) acids containing exogenous 2, 4 and 6 carbon units (M+2, M+4 and M+6) from [1,2-<sup>13</sup>C] acetate per unlabeled endogenous M+0 palmitic and stearic acids, respectively.

### **Knockdown of SREBPs**

siRNAs targeting *Srebp1*, *Srebp2*, and control siRNA were obtained from Sigma (SREBP1, 5'-CACAGGAGGACAUCUUGCUGCUUCU-3'; SREBP2, 5'-CGAGGAUCAUCCAGCAGCCUUUGAU-3'; control siRNA, 5'-UUCUCCGAACGUGUCACGU-3'). Fibroblasts were transfected with the siRNAs using TransIT-X2 Reagent (Mirus Bio LLC).

### **Hypothalamus isolation**

Isolation of the hypothalamus has been described previously (36). The hypothalami were homogenized using glass dounce tissue grinders, and the proteins were dissolved in an extraction buffer described above.

### **Visceral fat measurement**

16-week-old mice were euthanized by CO<sub>2</sub> inhalation. Epididymal, retroperitoneal, mesenteric and subcutaneous fat pads were carefully removed and weighted.

### **Leptin sensitivity test**

Individually housed mice were fasted for 18 h and injected with PBS by ip injection. Food intake was measured for following 24 h (Control). One week later, the same mice were fasted for 18 h and injected with 1 µg/g body weight of leptin by ip injection to test leptin sensitivity. Food intake was measured for following 24 h.

### **Preparation of plasma sample and leptin ELISA**

Individually housed mice were fasted for 18 h and peripheral blood was collected from the facial vein into 1.5 ml tube containing 1 µl of 0.5 M EDTA and centrifuged at 2000 rpm for 5 min. Supernatant was kept as plasma. Plasma leptin levels were measured using Leptin (mouse) ELISA kit (ENZO). The assay was conducted according to the manufactured protocols.

### **Measuring mouse body temperature**

Rectal temperature was measured using TCAT-2DF controller (Physitemp Instruments).

### **Intracerebroventricular injection of tunicamycin**

Intracerebroventricular injection of tunicamycin has described previously (40). Briefly, 8-week-old mice were anesthetized and 26 gauge syringes (Hamilton) were inserted into the third ventricle under stereotaxic control using stereotaxic apparatus (-1.8 mm anteroventral, 0.0 mm lateral, 5.0 mm dorsoventral from bregma). 20 µg of tunicamycin was injected over 5 min. After surgery, the head skin was sewed using surgical sutures (Henry Schein).

### **Electrophoresis mobility shift assay (EMSA)**

Oligonucleotides for the consensus NF- $\kappa$ B binding DNA site were purchased from Promega. The binding reaction contained <sup>32</sup>P radiolabeled oligonucleotide probe, 50 µg of tissue extracts, 4% glycerol, 1mM MgCl<sub>2</sub>, 0.5mM EDTA, 0.5 mM DTT, 50 mM NaCl, 10 mM Tris-HCl (pH 7.5), 500 ng of poly (dI-dC) (GE Healthcare), and 10 µg of bovine serum albumin to a final concentration of 15 µl. The reaction mixture were incubated at 25 °C for 30 min, separated by 5 % (w/v) polyacrylamide gel, and visualized by autoradiography.

### **Flow cytometric analysis**

Fibroblasts were fixed with 2% paraformaldehyde in PBS for 15 min at room temperature and analyzed by a flow cytometer (BD Bioscience LSR II). Data were analyzed using FlowJo software (Tree Star).

### **Statistical analyses**

Statistical analyses were performed using two-tailed Student's t test for comparing the means of two groups. \*,  $p < 0.05$ ; \*\*,  $p < 0.01$ ; \*\*\*,  $p < 0.001$ ; NS, not significant when  $p > 0.05$ .

## **ACKNOWLEDGEMENTS**

We thank NC State biological animal facility for technical support, Dr. Akira for *Tak1*-loxed mice, Dr. Valerie for electron microscopy analysis and Dr. Myers for providing LepRb-plasmid. This work was supported by National Institutes of Health Grant GM068812 (J.N-T) and NS062182 (H.T.G). The lipid flux study utilized Core Services supported by grant DK089503 of NIH to the University of Michigan.

## REFERENCES

1. Voeltz, G.K., Rolls, M.M., and Rapoport, T.A. 2002. Structural organization of the endoplasmic reticulum. *EMBO Rep* 3:944-950.
2. Sitia, R., and Braakman, I. 2003. Quality control in the endoplasmic reticulum protein factory. *Nature* 426:891-894.
3. Walter, P., and Ron, D. 2011. The unfolded protein response: from stress pathway to homeostatic regulation. *Science* 334:1081-1086.
4. Tabas, I., and Ron, D. 2011. Integrating the mechanisms of apoptosis induced by endoplasmic reticulum stress. *Nat Cell Biol* 13:184-190.
5. Lu, M., Lawrence, D.A., Marsters, S., Acosta-Alvear, D., Kimmig, P., Mendez, A.S., Paton, A.W., Paton, J.C., Walter, P., and Ashkenazi, A. 2014. Cell death. Opposing unfolded-protein-response signals converge on death receptor 5 to control apoptosis. *Science* 345:98-101.
6. Sakurai, H. 2012. Targeting of TAK1 in inflammatory disorders and cancer. *Trends Pharmacol Sci* 33:522-530.
7. Mihaly, S.R., Ninomiya-Tsuji, J., and Morioka, S. 2014. TAK1 control of cell death. *Cell Death Differ* 21:1667-1676.
8. Sato, S., Sanjo, H., Takeda, K., Ninomiya-Tsuji, J., Yamamoto, M., Kawai, T., Matsumoto, K., Takeuchi, O., and Akira, S. 2005. Essential function for the kinase TAK1 in innate and adaptive immune responses. *Nat Immunol* 6:1087-1095.
9. Omori, E., Matsumoto, K., Sanjo, H., Sato, S., Akira, S., Smart, R.C., and Ninomiya-Tsuji, J. 2006. TAK1 is a master regulator of epidermal homeostasis involving skin inflammation and apoptosis. *J Biol Chem* 281:19610-19617.

10. INOkuchi, S., Aoyama, T., Miura, K., Osterreicher, C.H., Kodama, Y., Miyai, K., Akira, S., Brenner, D.A., and Seki, E. 2010. Disruption of TAK1 in hepatocytes causes hepatic injury, inflammation, fibrosis, and carcinogenesis. *Proc Natl Acad Sci U S A* 107:844-849.
11. Bettermann, K., Vucur, M., Haybaeck, J., Koppe, C., Janssen, J., Heymann, F., Weber, A., Weiskirchen, R., Liedtke, C., Gassler, N., et al. 2010. TAK1 suppresses a NEMO-dependent but NF- $\kappa$ B-independent pathway to liver cancer. *Cancer Cell* 17:481-496.
12. Morioka, S., Inagaki, M., Komatsu, Y., Mishina, Y., Matsumoto, K., and Ninomiya-Tsuji, J. 2012. TAK1 kinase signaling regulates embryonic angiogenesis by modulating endothelial cell survival and migration. *Blood* 120:3846-3857.
13. Kajino-Sakamoto, R., Omori, E., Nighot, P.K., Blikslager, A.T., Matsumoto, K., and Ninomiya-Tsuji, J. 2010. TGF-beta-activated kinase 1 signaling maintains intestinal integrity by preventing accumulation of reactive oxygen species in the intestinal epithelium. *J Immunol* 185:4729-4737.
14. Morioka, S., Broglie, P., Omori, E., Ikeda, Y., Takaesu, G., Matsumoto, K., and Ninomiya-Tsuji, J. 2014. TAK1 kinase switches cell fate from apoptosis to necrosis following TNF stimulation. *J Cell Biol* 204:607-623.
15. Omori, E., Morioka, S., Matsumoto, K., and Ninomiya-Tsuji, J. 2008. TAK1 regulates reactive oxygen species and cell death in keratinocytes, which is essential for skin integrity. *J Biol Chem* 283:26161-26168.
16. Oyadomari, S., and Mori, M. 2004. Roles of CHOP/GADD153 in endoplasmic reticulum stress. *Cell Death Differ* 11:381-389.

17. Ron, D., and Walter, P. 2007. Signal integration in the endoplasmic reticulum unfolded protein response. *Nat Rev Mol Cell Biol* 8:519-529.
18. Wiest, D.L., Burkhardt, J.K., Hester, S., Hortsch, M., Meyer, D.I., and Argon, Y. 1990. Membrane biogenesis during B cell differentiation: most endoplasmic reticulum proteins are expressed coordinately. *J Cell Biol* 110:1501-1511.
19. Jackson, M.R., Nilsson, T., and Peterson, P.A. 1990. Identification of a consensus motif for retention of transmembrane proteins in the endoplasmic reticulum. *EMBO J* 9:3153-3162.
20. Sriburi, R., Jackowski, S., Mori, K., and Brewer, J.W. 2004. XBP1: a link between the unfolded protein response, lipid biosynthesis, and biogenesis of the endoplasmic reticulum. *J Cell Biol* 167:35-41.
21. Schuck, S., Prinz, W.A., Thorn, K.S., Voss, C., and Walter, P. 2009. Membrane expansion alleviates endoplasmic reticulum stress independently of the unfolded protein response. *J Cell Biol* 187:525-536.
22. Shimano, H. 2001. Sterol regulatory element-binding proteins (SREBPs): transcriptional regulators of lipid synthetic genes. *Prog Lipid Res* 40:439-452.
23. Morioka, S., Sai, K., Omori, E., Ikeda, Y., Matsumoto, K., and Ninomiya-Tsuji, J. 2015. TAK1 regulates hepatic lipid homeostasis through SREBP. *Oncogene* in press.
24. Kamisuki, S., Mao, Q., Abu-Elheiga, L., Gu, Z., Kugimiya, A., Kwon, Y., Shinohara, T., Kawazoe, Y., Sato, S., Asakura, K., et al. 2009. A small molecule that blocks fat synthesis by inhibiting the activation of SREBP. *Chem Biol* 16:882-892.
25. McLaughlin, L., Burchell, B., Pritchard, M., Wolf, C.R., and Friedberg, T. 1999. Treatment of mammalian cells with the endoplasmic

- reticulum-proliferator compactin strongly induces recombinant and endogenous xenobiotic metabolizing enzymes and 3-hydroxy-3-methylglutaryl-CoA reductase in vitro. *J Cell Sci* 112 ( Pt 4):515-523.
26. Poland, A., Mak, I., Glover, E., Boatman, R.J., Ebetino, F.H., and Kende, A.S. 1980. 1,4-Bis[2-(3,5-dichloropyridyloxy)]benzene, a potent phenobarbital-like inducer of microsomal monooxygenase activity. *Mol Pharmacol* 18:571-580.
27. Maiuolo, J., Bulotta, S., Verderio, C., Benfante, R., and Borgese, N. 2011. Selective activation of the transcription factor ATF6 mediates endoplasmic reticulum proliferation triggered by a membrane protein. *Proc Natl Acad Sci U S A* 108:7832-7837.
28. Griffiths, B., Lewis, C.A., Bensaad, K., Ros, S., Zhang, Q., Ferber, E.C., Konisti, S., Peck, B., Miess, H., East, P., et al. 2013. Sterol regulatory element binding protein-dependent regulation of lipid synthesis supports cell survival and tumor growth. *Cancer Metab* 1:3.
29. Glass, C.K., and Olefsky, J.M. 2012. Inflammation and lipid signaling in the etiology of insulin resistance. *Cell Metab* 15:635-645.
30. Tall, A.R., and Yvan-Charvet, L. 2015. Cholesterol, inflammation and innate immunity. *Nat Rev Immunol* 15:104-116.
31. Glass, C.K., and Witztum, J.L. 2001. Atherosclerosis. the road ahead. *Cell* 104:503-516.
32. Shaffer, A.L., Shapiro-Shelef, M., Iwakoshi, N.N., Lee, A.H., Qian, S.B., Zhao, H., Yu, X., Yang, L., Tan, B.K., Rosenwald, A., et al. 2004. XBP1, downstream of Blimp-1, expands the secretory apparatus and other organelles, and increases protein synthesis in plasma cell differentiation. *Immunity* 21:81-93.

33. Hetz, C., and Mollereau, B. 2014. Disturbance of endoplasmic reticulum proteostasis in neurodegenerative diseases. *Nat Rev Neurosci* 15:233-249.
34. Hotamisligil, G.S. 2010. Endoplasmic reticulum stress and the inflammatory basis of metabolic disease. *Cell* 140:900-917.
35. Ozcan, U., Yilmaz, E., Ozcan, L., Furuhashi, M., Vaillancourt, E., Smith, R.O., Gorgun, C.Z., and Hotamisligil, G.S. 2006. Chemical chaperones reduce ER stress and restore glucose homeostasis in a mouse model of type 2 diabetes. *Science* 313:1137-1140.
36. Zhang, X., Zhang, G., Zhang, H., Karin, M., Bai, H., and Cai, D. 2008. Hypothalamic IKKbeta/NF-kappaB and ER stress link overnutrition to energy imbalance and obesity. *Cell* 135:61-73.
37. Schneeberger, M., Dietrich, M.O., Sebastian, D., Imbernon, M., Castano, C., Garcia, A., Esteban, Y., Gonzalez-Franquesa, A., Rodriguez, I.C., Bortolozzi, A., et al. 2013. Mitofusin 2 in POMC neurons connects ER stress with leptin resistance and energy imbalance. *Cell* 155:172-187.
38. Woods, S.C., Seeley, R.J., Porte, D., Jr., and Schwartz, M.W. 1998. Signals that regulate food intake and energy homeostasis. *Science* 280:1378-1383.
39. Myers, M.G., Cowley, M.A., and Munzberg, H. 2008. Mechanisms of leptin action and leptin resistance. *Annu Rev Physiol* 70:537-556.
40. Ozcan, L., Ergin, A.S., Lu, A., Chung, J., Sarkar, S., Nie, D., Myers, M.G., Jr., and Ozcan, U. 2009. Endoplasmic reticulum stress plays a central role in development of leptin resistance. *Cell Metab* 9:35-51.
41. Won, J.C., Jang, P.G., Namkoong, C., Koh, E.H., Kim, S.K., Park, J.Y., Lee, K.U., and Kim, M.S. 2009. Central administration of an

- endoplasmic reticulum stress inducer inhibits the anorexigenic effects of leptin and insulin. *Obesity (Silver Spring)* 17:1861-1865.
42. Engin, F., and Hotamisligil, G.S. 2010. Restoring endoplasmic reticulum function by chemical chaperones: an emerging therapeutic approach for metabolic diseases. *Diabetes Obes Metab* 12 Suppl 2:108-115.
43. Cohen, F.E., and Kelly, J.W. 2003. Therapeutic approaches to protein-misfolding diseases. *Nature* 426:905-909.
44. Aridor, M. 2007. Visiting the ER: the endoplasmic reticulum as a target for therapeutics in traffic related diseases. *Adv Drug Deliv Rev* 59:759-781.
45. Fu, S., Yalcin, A., Lee, G.Y., Li, P., Fan, J., Arruda, A.P., Pers, B.M., Yilmaz, M., Eguchi, K., and Hotamisligil, G.S. 2015. Phenotypic assays identify azoramide as a small-molecule modulator of the unfolded protein response with antidiabetic activity. *Sci Transl Med* 7:292ra298.
46. Liu, J., Lee, J., Salazar Hernandez, M.A., Mazitschek, R., and Ozcan, U. 2015. Treatment of obesity with celastrol. *Cell* 161:999-1011.
47. Cai, D. 2013. Neuroinflammation and neurodegeneration in overnutrition-induced diseases. *Trends Endocrinol Metab* 24:40-47.
48. Lindholm, D., Wootz, H., and Korhonen, L. 2006. ER stress and neurodegenerative diseases. *Cell Death & Differentiation* 13:385-392.
49. Oswal, A., and Yeo, G. 2010. Leptin and the control of body weight: a review of its diverse central targets, signaling mechanisms, and role in the pathogenesis of obesity. *Obesity (Silver Spring)* 18:221-229.
50. Zimmerman, L., Parr, B., Lendahl, U., Cunningham, M., McKay, R., Gavin, B., Mann, J., Vassileva, G., and McMahon, A. 1994. Independent regulatory elements in the nestin gene direct transgene expression to neural stem cells or muscle precursors. *Neuron* 12:11-24.

51. Liang, H., Hippenmeyer, S., and Ghashghaei, H.T. 2012. A Nestin-cre transgenic mouse is insufficient for recombination in early embryonic neural progenitors. *Biol Open* 1:1200-1203.
52. Goldmann, T., Wieghofer, P., Muller, P.F., Wolf, Y., Varol, D., Yona, S., Brendecke, S.M., Kierdorf, K., Staszewski, O., Datta, M., et al. 2013. A new type of microglia gene targeting shows TAK1 to be pivotal in CNS autoimmune inflammation. *Nat Neurosci* 16:1618-1626.
53. Harno, E., Cottrell, E.C., and White, A. 2013. Metabolic pitfalls of CNS Cre-based technology. *Cell Metab* 18:21-28.
54. Sabio, G., Cavanagh-Kyros, J., Barrett, T., Jung, D.Y., Ko, H.J., Ong, H., Morel, C., Mora, A., Reilly, J., Kim, J.K., et al. 2010. Role of the hypothalamic-pituitary-thyroid axis in metabolic regulation by JNK1. *Genes Dev* 24:256-264.
55. Tsaousidou, E., Paeger, L., Belgardt, B.F., Pal, M., Wunderlich, C.M., Bronneke, H., Collienne, U., Hampel, B., Wunderlich, F.T., Schmidt-Supprian, M., et al. 2014. Distinct Roles for JNK and IKK Activation in Agouti-Related Peptide Neurons in the Development of Obesity and Insulin Resistance. *Cell Rep* 9:1495-1506.
56. del Barco Barrantes, I., Coya, J.M., Maina, F., Arthur, J.S., and Nebreda, A.R. 2011. Genetic analysis of specific and redundant roles for p38alpha and p38beta MAPKs during mouse development. *Proc Natl Acad Sci U S A* 108:12764-12769.
57. Sabapathy, K., Kallunki, T., David, J.P., Graef, I., Karin, M., and Wagner, E.F. 2001. c-Jun NH2-terminal kinase (JNK)1 and JNK2 have similar and stage-dependent roles in regulating T cell apoptosis and proliferation. *J Exp Med* 193:317-328.

58. Voisin, L., Saba-El-Leil, M.K., Julien, C., Fremin, C., and Meloche, S. 2010. Genetic demonstration of a redundant role of extracellular signal-regulated kinase 1 (ERK1) and ERK2 mitogen-activated protein kinases in promoting fibroblast proliferation. *Mol Cell Biol* 30:2918-2932.
59. Neubert, M., Ridder, D.A., Bargiotas, P., Akira, S., and Schwaninger, M. 2011. Acute inhibition of TAK1 protects against neuronal death in cerebral ischemia. *Cell Death Differ* 18:1521-1530.
60. Zhang, D., Hu, Y., Sun, Q., Zhao, J., Cong, Z., Liu, H., Zhou, M., Li, K., and Hang, C. 2013. Inhibition of transforming growth factor beta-activated kinase 1 confers neuroprotection after traumatic brain injury in rats. *Neuroscience* 238:209-217.
61. Hotamisligil, G.S. 2006. Inflammation and metabolic disorders. *Nature* 444:860-867.
62. Kim, I., Xu, W., and Reed, J.C. 2008. Cell death and endoplasmic reticulum stress: disease relevance and therapeutic opportunities. *Nat Rev Drug Discov* 7:1013-1030.
63. Minamino, T., and Kitakaze, M. 2010. ER stress in cardiovascular disease. *J Mol Cell Cardiol* 48:1105-1110.
64. Zhang, K., and Kaufman, R.J. 2008. From endoplasmic-reticulum stress to the inflammatory response. *Nature* 454:455-462.
65. Thaler, J.P., Yi, C.X., Schur, E.A., Guyenet, S.J., Hwang, B.H., Dietrich, M.O., Zhao, X., Sarruf, D.A., Izgur, V., Maravilla, K.R., et al. 2012. Obesity is associated with hypothalamic injury in rodents and humans. *J Clin Invest* 122:153-162.
66. Tronche, F., Kellendonk, C., Kretz, O., Gass, P., Anlag, K., Orban, P.C., Bock, R., Klein, R., and Schutz, G. 1999. Disruption of the

glucocorticoid receptor gene in the nervous system results in reduced anxiety. *Nat Genet* 23:99-103.

67. Ninomiya-Tsuji, J., Kishimoto, K., Hiyama, A., INOue, J., Cao, Z., and Matsumoto, K. 1999. The kinase TAK1 can activate the NIK-I kappaB as well as the MAP kinase cascade in the IL-1 signalling pathway. *Nature* 398:252-256.

## **FIGURES**

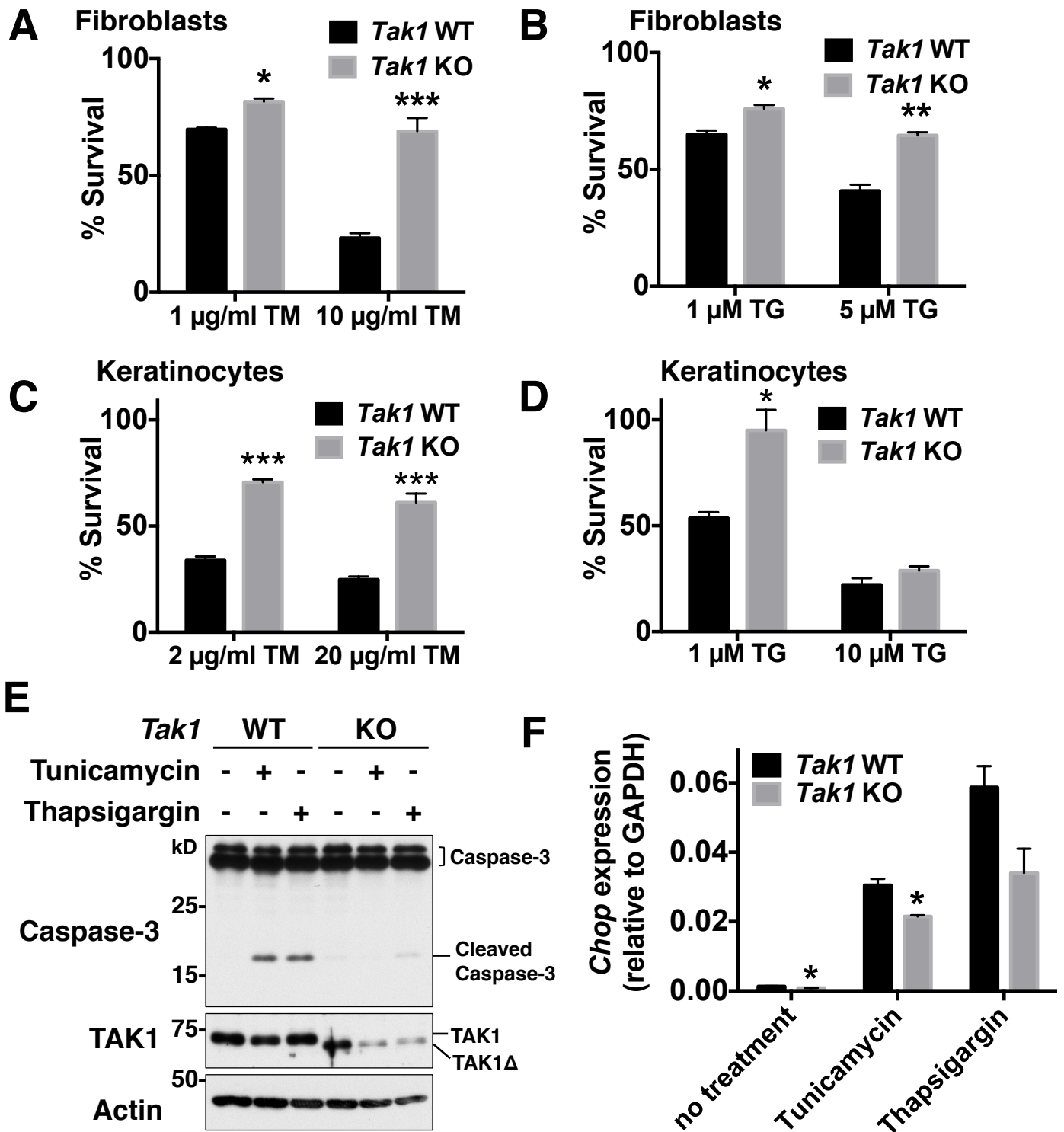


**Figure 1 | *Tak1*-deficiency protects cells from ER stress-induced cell death**

(A-D) *Tak1* wild-type (*Tak1* WT) and *Tak1*-deficient (*Tak1* KO) fibroblasts (A, B) or keratinocytes (C, D) were seeded on 24-well plates and treated with vehicle (DMSO) alone or the indicated concentrations of tunicamycin (TM) or thapsigargin (TG) for 18 h. Cell viability was measured by crystal violet staining.  $n = 3$  per treatment; mean  $\pm$  s.e.m.; \*,  $p < 0.05$ ; \*\*,  $p < 0.01$ ; \*\*\*,  $p < 0.001$ . (E) *Tak1* WT and *Tak1* KO fibroblasts were treated with vehicle alone, 10  $\mu$ g/ml tunicamycin or 5  $\mu$ M thapsigargin for 24 h. Caspase-3 and TAK1 were analyzed by immunoblotting. Cleaved Caspase-3 and a truncated form of TAK1 (TAK1 $\Delta$ ) are indicated. In our *Tak1*-floxed system, TAK1 $\Delta$  lacking a small deletion of the ATP binding site is generated but TAK1 $\Delta$  protein is unstable and unfunctional (8).  $\beta$ -actin is shown as a loading control. (F) *Tak1* WT and *Tak1* KO fibroblasts were treated with 0.5  $\mu$ g/ml of tunicamycin or 0.1  $\mu$ M thapsigargin for 18 h. The mRNA level of *Chop* was analyzed by quantitative real-time PCR. mRNA level of *Chop* was quantified relative to *Gapdh* gene expression.  $n = 3$  per genotype; mean  $\pm$  s.e.m.; \*,  $p < 0.05$ .

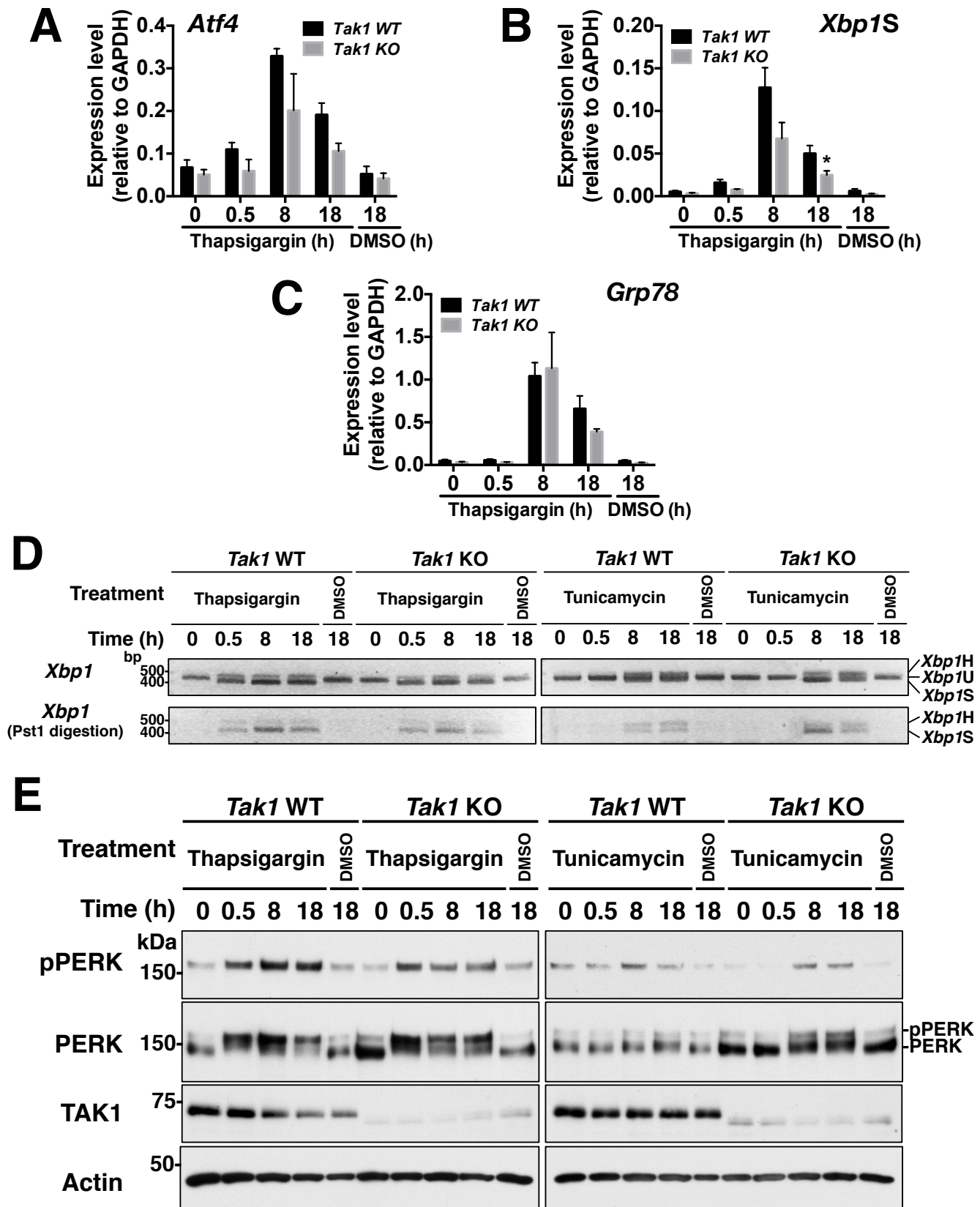


**Figure. 2 | *Tak1* deficiency does not alter UPR**

*Tak1* wild-type (*Tak1* WT) and *Tak1*-deficient (*Tak1* KO) fibroblasts were treated with 0.5  $\mu$ g/ml of tunicamycin (TM) or 0.1  $\mu$ M thapsigargin (TG) for the indicated time periods. **(A-C)** The mRNA levels of *Atf4* (A), Spliced form of *Xbp1* (*Xbp1S*) (B) and *Grp78* (C) were analyzed by quantitative real-time PCR.  $n = 3$  per genotype; mean  $\pm$  s.e.m.; \*,  $p < 0.05$ . **(D)** Unspliced *Xbp1* (*Xbp1U*) and spliced *Xbp1* (*Xbp1S*) were amplified by PCR. Hybrid of spliced and unspliced *Xbp1* fragments (*Xbp1H*) was also detected. To confirm the spliced *Xbp1* DNA fragments, PCR products were digested with Pst I, which digests only unspliced but not spliced or hybrid *Xbp1* DNA fragment (lower panel). **(E)** PERK phosphorylation was detected by immunoblotting. Total protein amounts of PERK, TAK1 and  $\beta$ -actin were also shown.

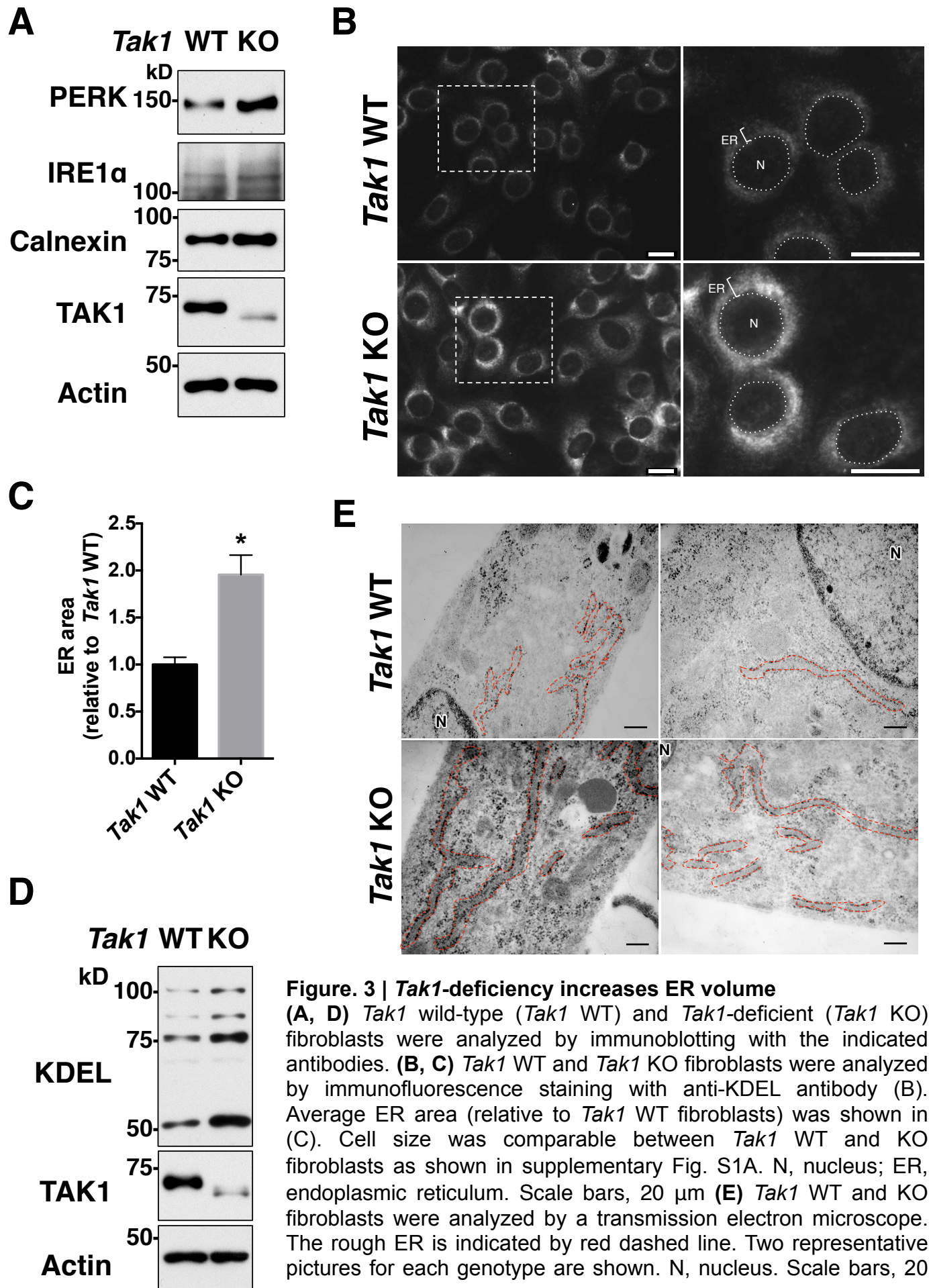


**Figure. 3 | *Tak1*-deficiency increases ER volume**

(A, D) *Tak1* wild-type (*Tak1* WT) and *Tak1*-deficient (*Tak1* KO) fibroblasts were analyzed by immunoblotting with the indicated antibodies. (B, C) *Tak1* WT and *Tak1* KO fibroblasts were analyzed by immunofluorescence staining with anti-KDEL antibody (B). Average ER area (relative to *Tak1* WT fibroblasts) was shown in (C). Cell size was comparable between *Tak1* WT and KO fibroblasts as shown in supplementary Fig. S1A. N, nucleus; ER, endoplasmic reticulum. Scale bars, 20  $\mu$ m (E) *Tak1* WT and KO fibroblasts were analyzed by a transmission electron microscope. The rough ER is indicated by red dashed line. Two representative pictures for each genotype are shown. N, nucleus. Scale bars, 20 nm.

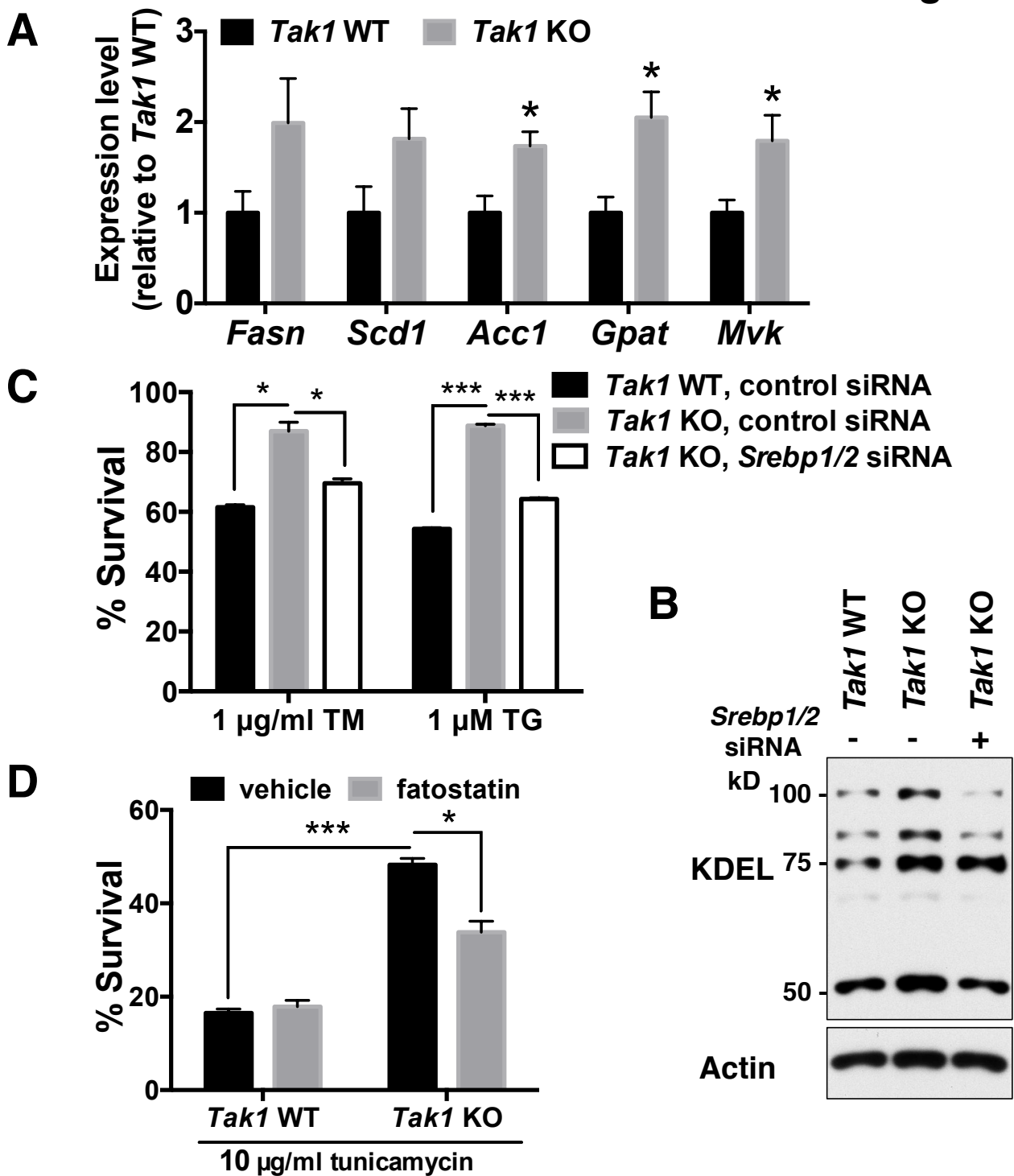


**Figure 4 | *Tak1*-deficiency enhances ER stress tolerance through SREBPs**

(A) mRNA levels of SREBP target genes in *Tak1* wild-type (*Tak1* WT) and *Tak1*-deficient (*Tak1* KO) fibroblasts were analyzed by quantitative real-time PCR. All mRNA levels were quantified relative to *Gapdh* gene expression and presented as fold change relative to *Tak1* WT fibroblasts. *Fasn*, fatty acid synthase; *Scd1*, stearyl coenzyme-A desaturase1; *Acc1*, acetyl-CoA carboxylase1; *Gpat*, glycerol-3-phosphate acyltransferase; *Mvk*, mevalonate kinase; n = 6 per genotype; mean  $\pm$  s.e.m.; \*, p < 0.05; \*\*, p < 0.01; \*\*\*, p < 0.001. (B, C) *Tak1* WT and *Tak1* KO fibroblasts were transfected with non-targeted control siRNA or a mixture of *Sreb1* and *Sreb2* siRNAs. At 72 h-post transfection, cell lysates were analyzed by immunoblotting with anti-KDEL antibody (B). Alternatively, at 72 h-post transfection, cells were treated with vehicle alone, 1 µg/ml tunicamycin (TM) or 1 µM thapsigargin (TG) for 18 h. Cell viability was measured by crystal violet staining (C). Expression levels of *Sreb1* and *Sreb2* were effectively downregulated by the transfection of siRNAs (supplementary Fig. S1D). n = 3 per treatment; mean  $\pm$  s.e.m.; \*, p < 0.05; \*\*, p < 0.01. (D) *Tak1* WT and *Tak1* KO fibroblasts were pre-treated with vehicle alone or 10 µg/ml of fatostatin for 24 h. Cells were then treated with either vehicle or 10 µg/ml tunicamycin (TM) for 18 h. Cell viability was measured by crystal violet staining. n = 3 per treatment; mean  $\pm$  s.e.m.; \*, p < 0.05; \*\*, p < 0.01.

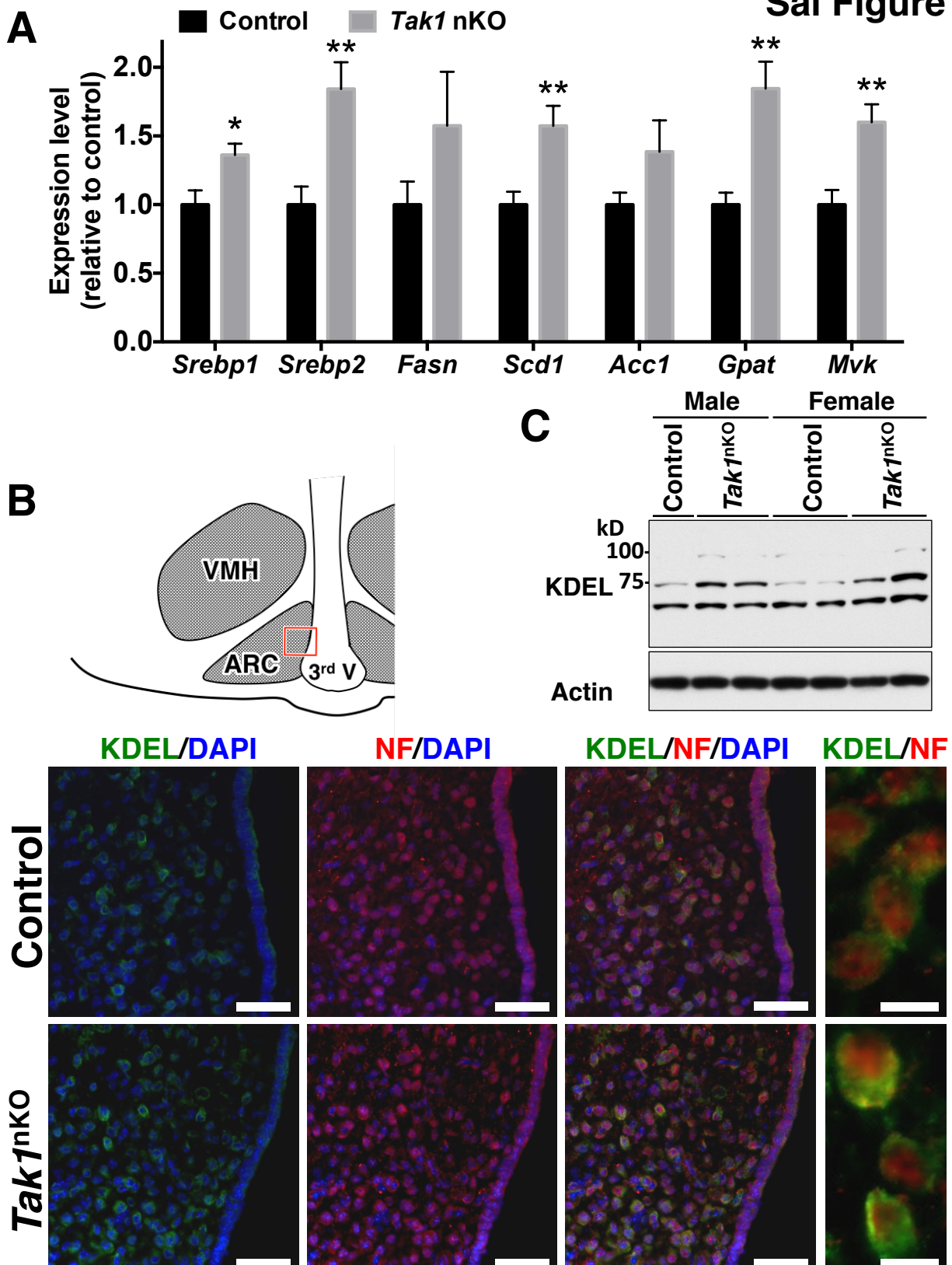


**Figure. 5 | CNS-specific deletion of *Tak1* activates SREBPs and induces ER expansion in the hypothalamus**

(A) mRNA levels of SREBP target genes in control and *Tak1*nKO hypothalamus from 8-week-old mice were analyzed by quantitative real-time PCR. All mRNA levels were quantified relative to *Gapdh* gene expression and presented as fold change relative to control mice. Control, n = 6; *Tak1* nKO, n = 4; mean  $\pm$  s.e.m.; \*, p < 0.05. (B) The arcuate nucleus (ARC) of the hypothalamic sections from 8-week-old control and *Tak1*nKO male mice were analyzed by immunofluorescence staining with anti-KDEL antibody (green), anti-neurofilament 200 (red) and DAPI (blue). The schematic diagram indicates the region of ARC shown in the pictures. ARC, arcuate nucleus; VMH, ventromedial hypothalamic nucleus; 3rd V, the third ventricle. Scale bars, the left three panels, 50  $\mu$ m; the far right panels, 10  $\mu$ m. (C) The hypothalamic extract from 16-week-old control and *Tak1*nKO male (lanes 1-3) and female (lanes 4-7) mice fed HFD for 12 weeks were analyzed by immunoblotting with anti-KDEL motif antibody. Each lane represents an individual mouse.

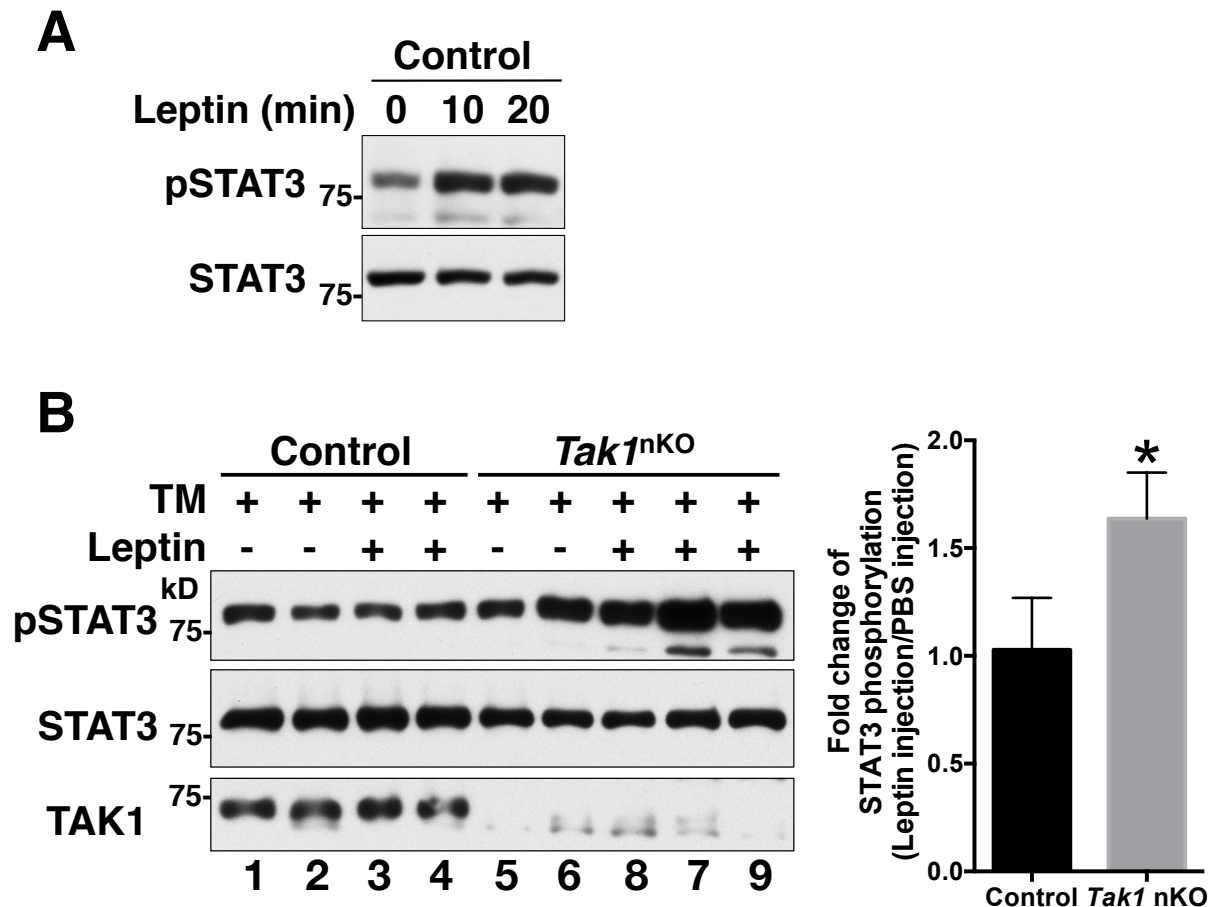


**Figure. 6 | CNS-specific deletion of *Tak1* protects mice against ER stress-induced leptin resistance**

(A) I.p injection of leptin induces STAT3 phosphorylation in the hypothalamus. Normal diet (ND)-fed 16-week-old control mice were fasted for 18 h. PBS or 1  $\mu$ g/g body weight of leptin were injected intraperitoneally and the hypothalamus was isolated at the indicated time points after injection. STAT3 phosphorylation was analyzed by immunoblotting. (B) 8-week-old control and *Tak1*<sup>nKO</sup> mice (ND-fed) were fasted for 12 h. 20  $\mu$ g of tunicamycin was injected by intracerebroventricular injection. After 6 h, vehicle (PBS) or 1  $\mu$ g/g body weight of leptin was injected intraperitoneally and hypothalamic STAT3 phosphorylation at 15 minutes-post injection was analyzed by immunoblotting. Total STAT3 and TAK1 proteins are also shown. Each lane represents an individual mouse. The graph (at right) shows the quantification of phospho-STAT3 intensities normalized to total STAT3 including data from additional samples not shown in the immunoblotting. Control, n = 4; *Tak1* nKO, n = 3; mean  $\pm$  s.e.m; \*, p < 0.05.

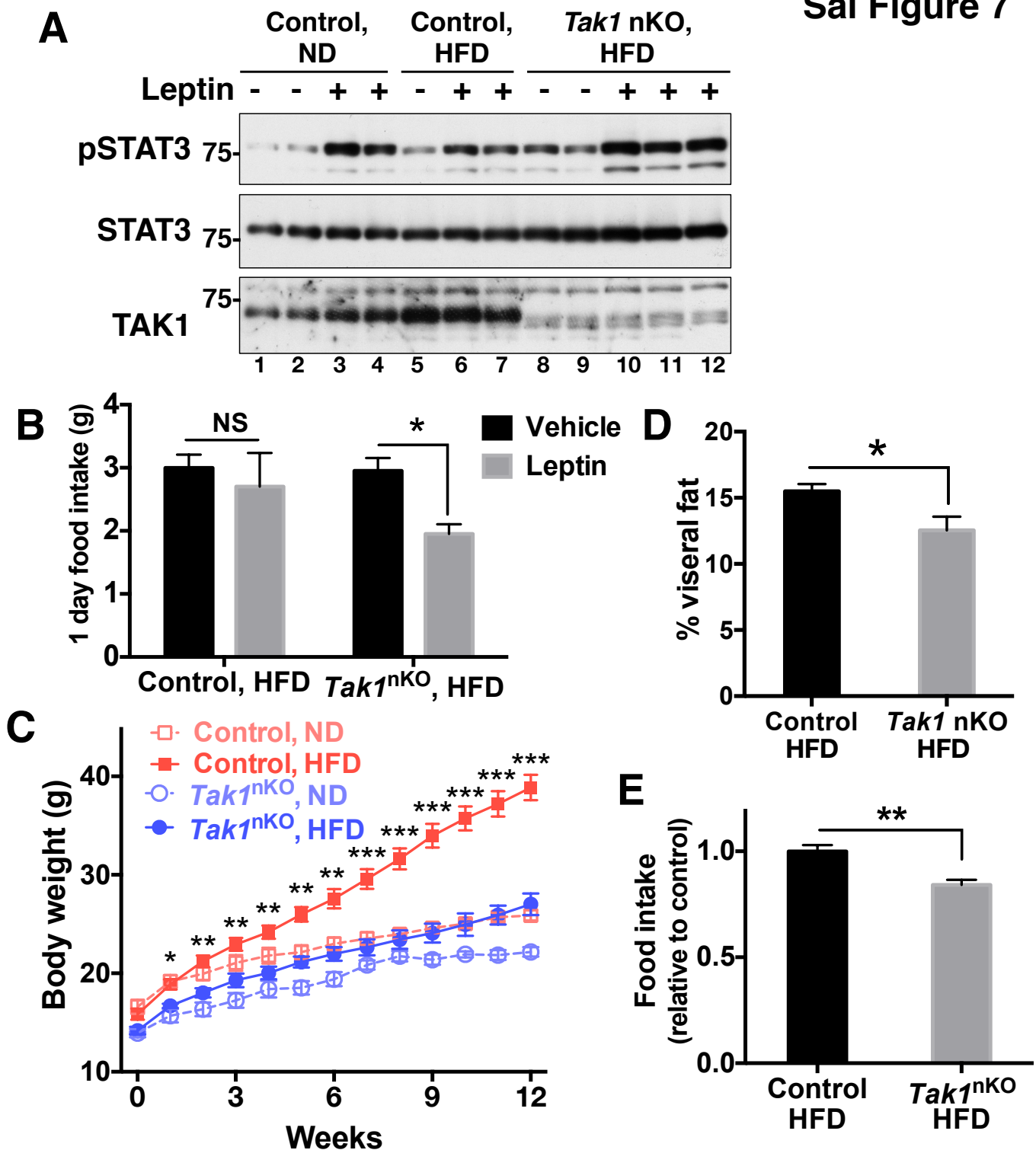
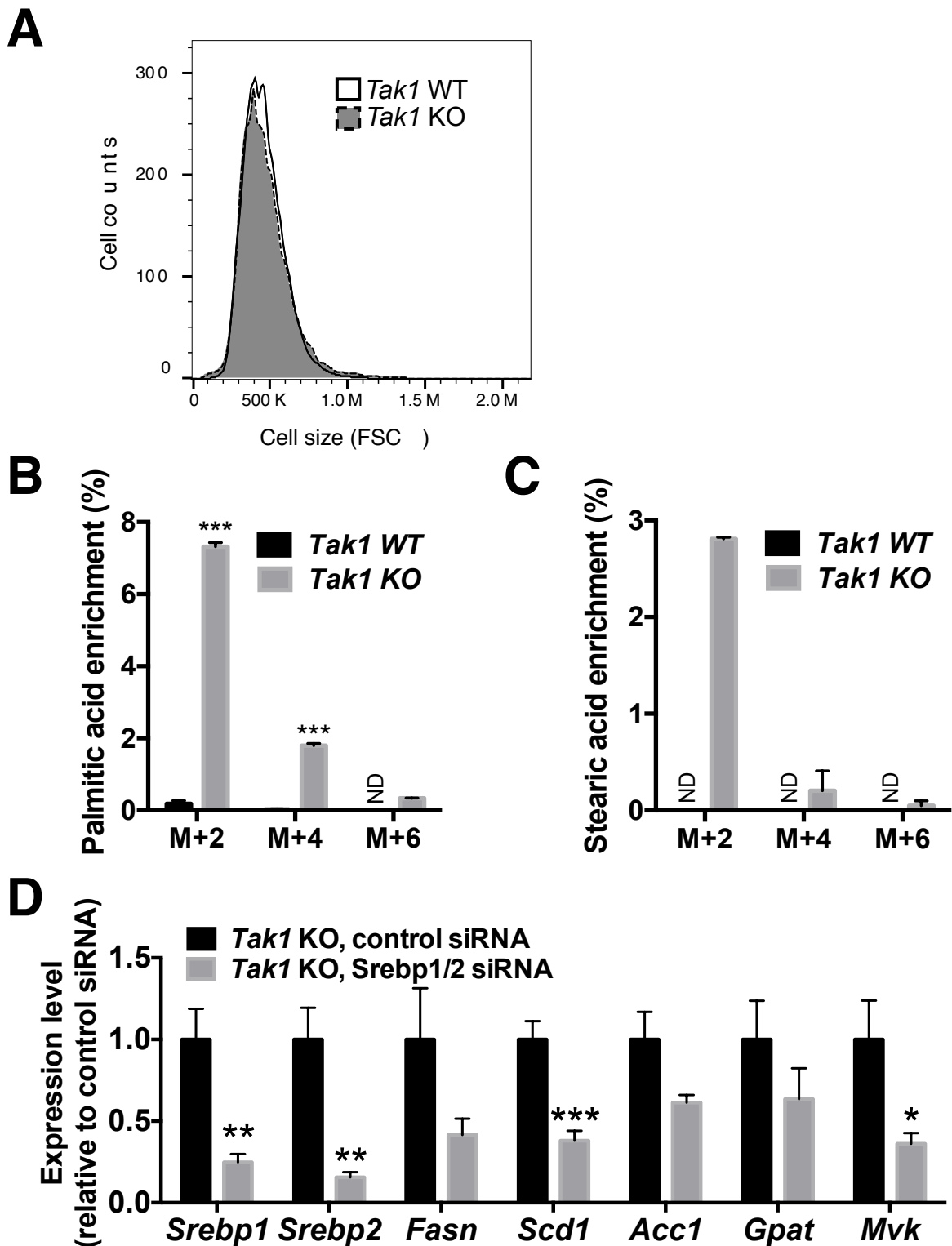


**Figure. 7 | CNS-specific deletion of *Tak1* protects mice from HFD-induced leptin resistance and obesity**

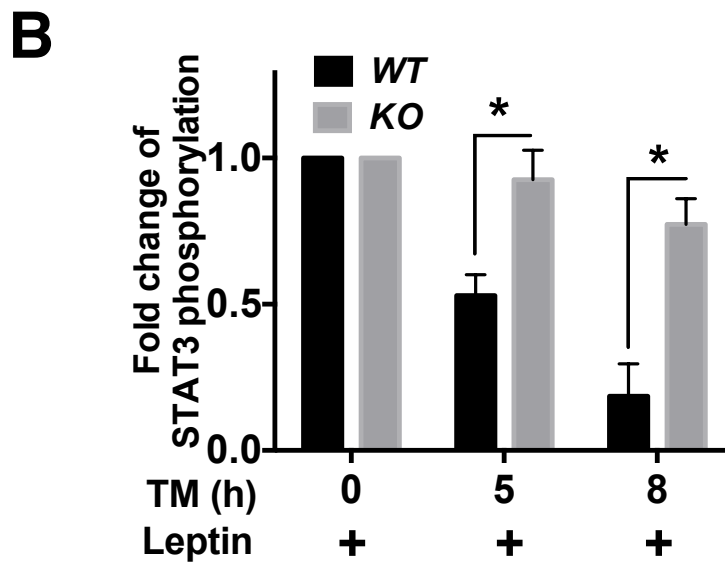
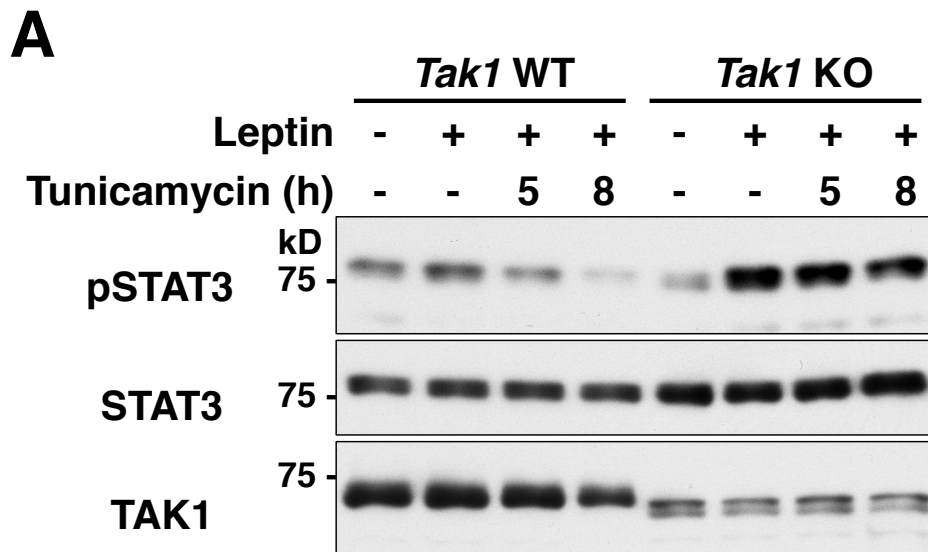
(A, B) 12 weeks ND fed control (control, ND), 12 weeks HFD-fed control (Control, HFD) and *Tak1*nKO (*Tak1*nKO, HFD) mice were fasted for 18 h. PBS or 1  $\mu$ g/g body weight of leptin were injected intraperitoneally. (A) The hypothalamus was isolated at 15 min-post injection and STAT3 phosphorylation was analyzed by immunoblotting. Each lane represents an individual mouse. (B) Food intake for 24 h after leptin injection was measured. Control with HFD; n = 5; *Tak1*nKO with HFD; n = 6; NS, not significant; \*, p < 0.05. (C-E) 4-week-old control and *Tak1*nKO male mice were fed either normal diet (ND) or high-fat diet (HFD) for 12 weeks. (C) Mice were weighed weekly. Control with ND, n = 4; control with HFD; n = 17; *Tak1*nKO with ND; n = 4; *Tak1*nKO with HFD; n = 6; p values shown are the comparison between control with HFD and *Tak1*nKO with HFD; \*, p < 0.05; \*\*, p < 0.01; \*\*\*, p < 0.001. Control mice include wild-type (*Tak1*<sup>flox/flox</sup> no-Cre) and *Tak1*<sup>flox/+</sup> *Nestin*-Cre mice. (D) Visceral fats were isolated and weighted at the end of experiment of (A). n = 4 per group; \*, p < 0.05. (E) At 11 weeks after ND or HFD feeding, Food intake was measured daily and cumulative food intake for 1 week was calculated. Control with HFD; n = 9; *Tak1*nKO with HFD; n = 5; \*\*, p < 0.01.

# Sai Supplementary Figure S1



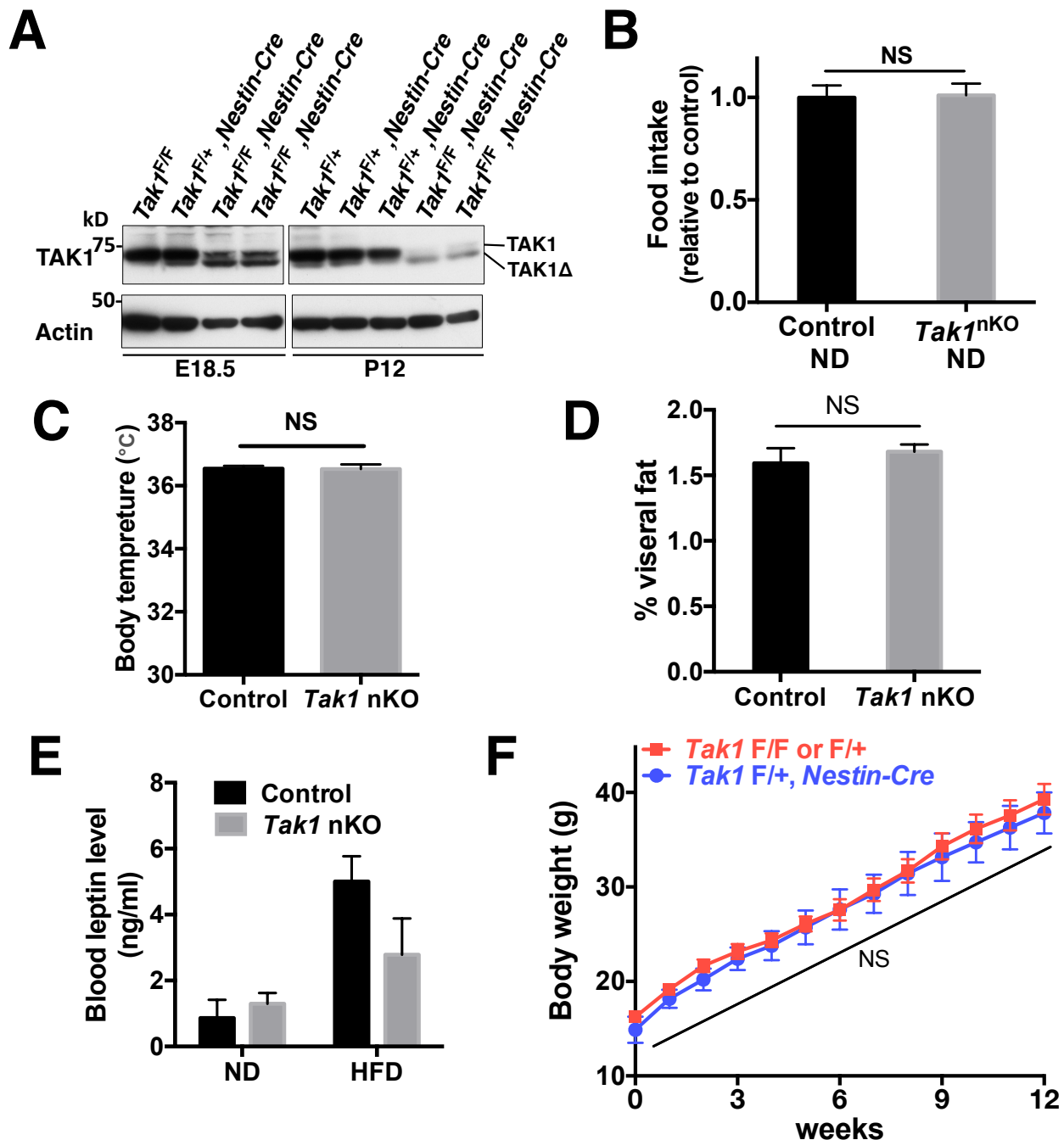
## Supplementary Figure S1 | Characterization of *Tak1*-deficient cells

(A) Cell size of *Tak1* WT and *Tak1* KO fibroblasts were analyzed by measuring forward scatter (FSC) using flow cytometry. (B, C) Contribution of de novo lipogenesis to palmitic and stearic acids. *Tak1* WT and *Tak1* KO fibroblasts were cultured with <sup>13</sup>C-acetate for 12 hours, and M+2, M+4 and M+6 enrichments of palmitic acid (B) and stearic acid (C) were determined by fluxomics analysis. ND, not detected; n = 3 per genotype; mean ± s.e.m; \*\*\*, p < 0.001. (D) *Srebps* siRNAs effectively downregulated mRNA levels of *Srebps* and their target genes. *Tak1*-deficient (*Tak1* KO) fibroblasts were transfected with non-targeted control siRNA or a mixture of *Srebp1* and *Srebp2* siRNAs. At 72 h-post transfection, mRNA levels of *Srebps* and SREBP target genes were analyzed by quantitative real-time PCR. All mRNA levels were quantified relative to *Gapdh* gene expression and presented as fold change relative to control siRNA-treated fibroblasts. *Fasn*, fatty acid synthase; *Scd1*, stearyl coenzyme-A desaturase1; *Acc1*, acetyl-CoA carboxylase1; *Gpat*, glycerol-3-phosphate acyltransferase; *Mvk*, mevalonate kinase; n = 6 per genotype; mean ± s.e.m; \*, p < 0.05; \*\*, p < 0.01; \*\*\*, p < 0.001.



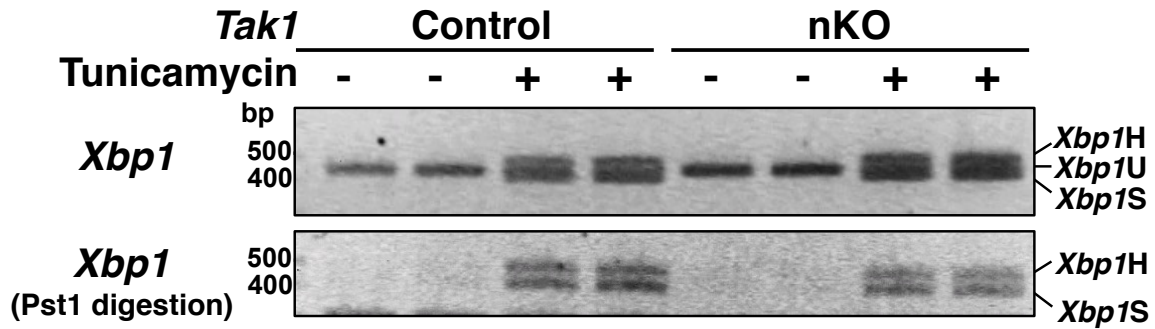
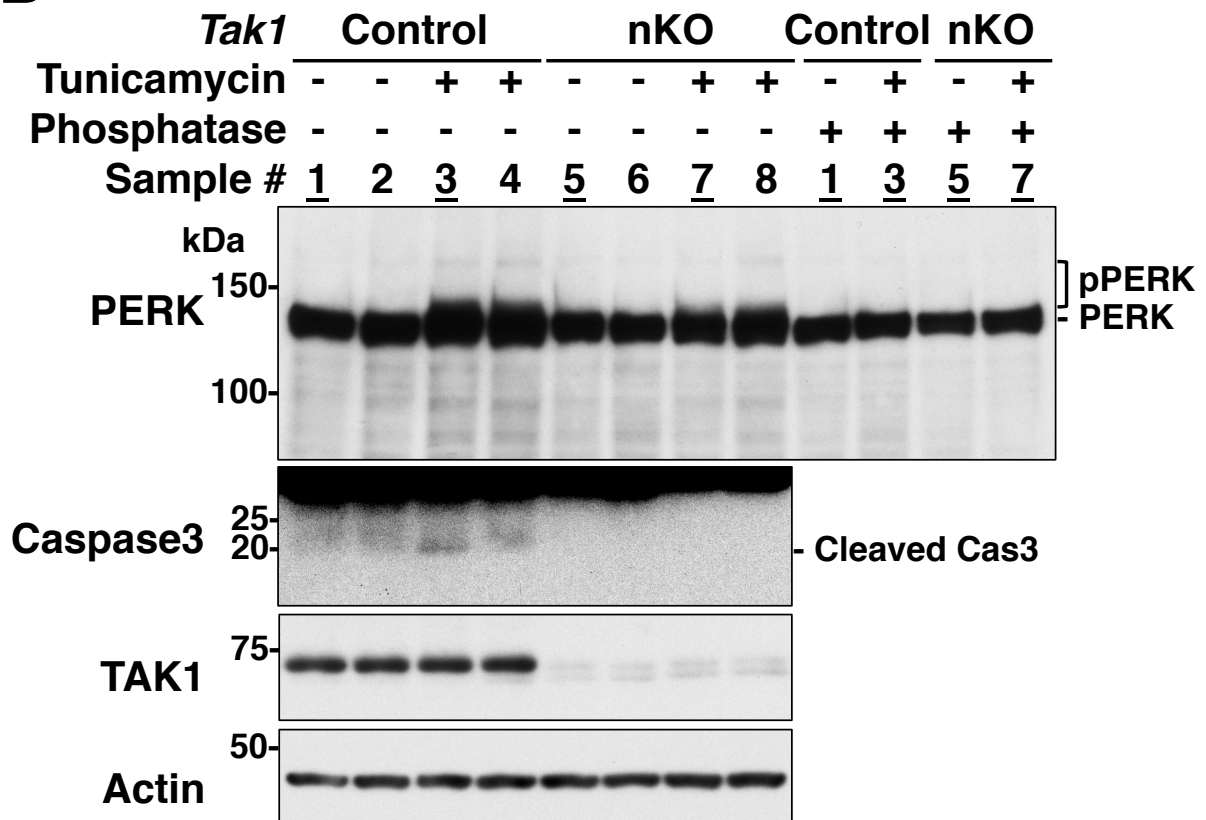
**Supplementary Figure S2 | *Tak1* deletion protects cells from ER stress-induced leptin resistance**

(A, B) *Tak1* deletion protects cells from ER stress-induced leptin resistance. Leptin receptor b-expressing wild-type (WT) or *Tak1*-deficient (KO) fibroblasts were treated with tunicamycin (TM) for the indicated time periods, and subsequently stimulated with leptin. Cells were harvested at 30 min-post leptin treatment and STAT3 phosphorylation was analyzed by immunoblotting. (A) The immunoblotting images are representative from four independent experiments. (B) The graph shows quantification of the intensities of phospho-STAT3 normalized to total STAT3 in four independent experiments.  $n = 4$  per treatment; mean  $\pm$  s.e.m; \*,  $p < 0.05$ .

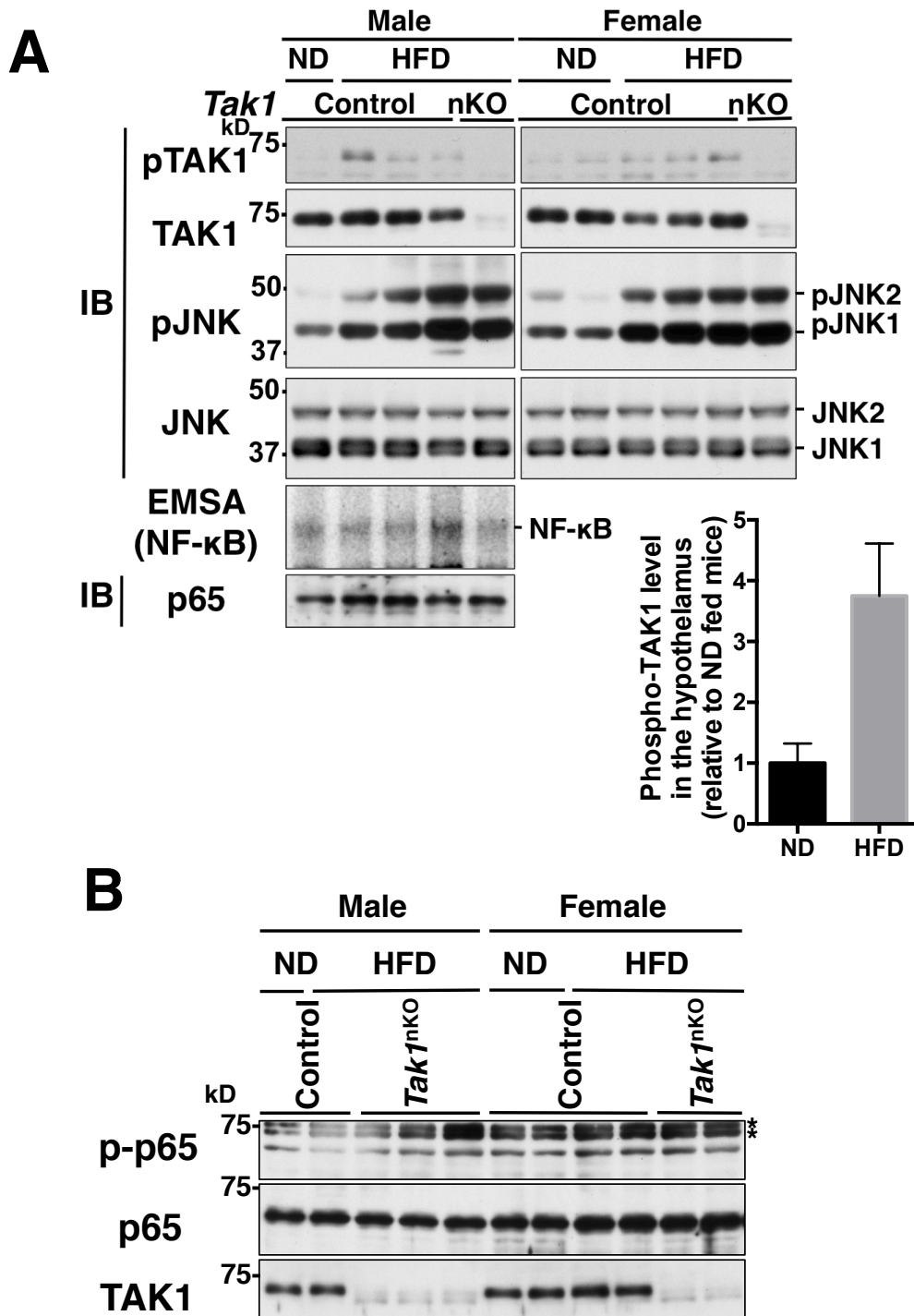


**Supplementary Figure S3 | Characterization of *Tak1* nKO mice**

**(A)** Protein levels of TAK1 in the brain of no-Cre, CNS-specific heterozygous *Tak1* deletion (*Nestin-Cre Tak1<sup>flx/+</sup>*) and CNS-specific homozygous *Tak1* deletion (*Nestin-Cre Tak1<sup>flx/flx</sup>*, refers to as *Tak1<sup>nKO</sup>* elsewhere) mice. Whole brain extracts at embryonic day 18.5 (E18.5) and postnatal day 12 (P12) from mice with the indicated genotype were analyzed by immunoblotting with TAK1 antibodies. Each lane represents an individual mouse. **(B-D)** Cumulative food intake for 1 week (B; n = 4 per genotype), rectal temperature (C; control, n = 5; *Tak1* nKO, n = 3) and percentage of visceral fat (D; control, n = 5; *Tak1* nKO, n = 3) of 8-week-old control and *Tak1<sup>nKO</sup>* male mice fed normal diet were measured. The data were presented as fold change relative to control mice. NS, not significant. **(E)** Plasma was collected from 8-week-old mice fed ND (8 weeks) or HFD (4 weeks). Circulating leptin levels were determined by ELISA. ND fed Control, n = 5; ND fed *Tak1* nKO, n = 3; HFD fed Control, n = 4; HFD fed *Tak1* nKO, n = 4; ND fed Control vs ND fed *Tak1* nKO, p = 0.595, HFD fed Control vs HFD fed *Tak1* nKO, p = 0.149. **(F)** 4-week-old wild-type (*Tak1<sup>Flox/+</sup>* or *Tak1<sup>Flox/Flox</sup>*) and heterozygous CNS *Tak1* deletion (*Tak1<sup>Flox/+</sup>, Nestin-Cre*) male mice were fed HFD for 12 weeks. Mice were weighed weekly. wild-type, n = 12; heterozygous CNS *Tak1* deletion *Tak1<sup>F/+</sup>, Nestin-Cre*; n = 5; NS, not significant.

**A****B****Supplementary Figure S4 | UPR analysis in the hypothalamus of *Tak1* nKO mice**

8-week-old control and *Tak1*nKO mice (ND-fed) were fasted for 12 h. Vehicle (DMSO, -) or 20  $\mu$ g of tunicamycin (+) was injected by intracerebroventricular injection. **(A)** Unspliced *Xbp1* (*Xbp1U*) and spliced *Xbp1* (*Xbp1S*) were amplified by PCR. Hybrid of spliced and unspliced XBP1 fragments (*Xbp1H*) was also detected. To confirm splicing of *Xbp1*, PCR products were incubated with Pst I restriction enzyme, which specifically digests unspliced XBP1 (lower panel). **(B)** PERK phosphorylation upon tunicamycin injection was determined by retarded migration of PERK on SDS-PAGE. Some protein extracts (indicated by underlined sample numbers) were incubated in the absence (-) or presence (+) of antarctic phosphatase at 30 °C for 30 min. The samples were immunoblotted with anti-PERK antibody. Phosphatase treatment completely diminished the retarded migration of PERK in tunicamycin injected samples, confirming that the migration shift is due to PERK phosphorylation. Caspase-3 cleavage was determined by immunoblotting. Protein amounts of TAK1 and  $\beta$ -actin were also shown.



**Supplementary Figure S5 | CNS-specific deletion of *Tak1* does not alter activities of JNK and NF-κB**

(A, B) 4-week-old control and *Tak1*<sup>nKO</sup> male (left panels) and female (right panels) mice were fed HFD for 12 weeks. Hypothalamic extracts were analyzed by immunoblotting (IB) with the indicated antibodies. The activity of NF-κB was measured by electrophoretic mobility shift assay (EMSA). Each lane represents an individual mouse. \*, non-specific bands. The graph (at bottom) shows the quantification of the intensities of phospho-TAK1 normalized to total TAK1 in the hypothalamus of ND or HFD-fed mice (relative to ND fed mice). ND, n = 3; HFD, n = 6, p = 0.069.